DESIGN OF COLD-FORMED HIGH STRENGTH STEEL SQUARE AND RECTANGULAR HOLLOW SECTION BEAM-COLUMNS

Jia-Lin Ma[1], Madhup Pandey[2,*], Tak-Ming Chan[3] and Ben Young[3]

[1]*Building Research Center, Vanke Co. Ltd., Huanmei Road, Shenzhen, China.*
[2]*Department of Civil Engineering, University of Nottingham, Nottingham, United Kingdom.*
[3]*Department of Civil and Environmental Engineering, The Hong Kong Polytechnic University, Hong Kong, China.*

Abstract

Cold-formed high strength steel (CFHSS) square and rectangular hollow section (SHS and RHS) beam-columns were investigated in this study with an objective to evaluate the applicability of existing design rules given in American, Australian and European codes for SHS and RHS beam-columns of S700, S900 and S1100 steel grades, and subsequently, provide economical and reliable design rule for CFHSS SHS and RHS beam-columns. A comprehensive numerical investigation was performed in this study, where the values of flat width-to-thickness ratio of the tubular sections ranged from 7.5 to 96. The constitutive model developed for CFHSS tubular members was used in the numerical investigation. Global and local geometric imperfections were also included in the numerical models. In total, 465 data were compared with the nominal capacities predicted from American, Australian and European codes, including 390 numerical data obtained in this investigation. The safety levels of design rules given in these standards were examined by performing a reliability analysis. It has been demonstrated that the current design rules given in the American, Australian and European codes provide conservative predictions. A modified design method based on the recommendations given in European code was proposed in this study. Overall, it has been proved that the proposed design rule provides accurate and reliable predictions for the design of cold-formed S700, S900 and S1100 steel grades SHS and RHS beam-columns.

Keywords: Beam-column; Cold-formed steel; Finite element; High strength steel; Hollow section; Tubular members.

*Corresponding author. (e-mail: madhup.pandey@nottingham.ac.uk)

1. Introduction

Cold-formed steel tubular (CST) members are increasingly used in several construction and infrastructure projects because of their high torsional strength, high strength-to-weight ratios, easy fabrication, and ability to fill the hollow space with concrete or other materials [1-9]. Recent years have seen tremendous growth in the steel manufacturing and fabrication sectors, leading to a significant increase in the production of high strength steels (HSS) of different steel grades. CFHSS hollow section members offer various unparallel merits compared to their normal strength steel (yield stress $\leq$ 460 MPa) counterparts, including high strength-to-weight ratio, reduced fabrication, handling and transportation expenses as well as reduced on-site erection time. In addition, due to the relatively reduced thickness of HSS members compared to identical normal strength steel members, the weld sizes and associated welding residual stresses are also reduced by an appreciable amount. Currently, the advantages of HSS material are mainly utilised by the automobile and aviation industries, and owing to the unavailability of appropriate design provisions, the applications of CFHSS tubular members in the construction sector are quite limited. With an aim to propose accurate and reliable design rules for tubular members and joints made of S690 to S1100 steel grades, several studies had been conducted to investigate the material properties of CFHSS tubular members [3,10], structural behaviour of CFHSS tubular stub columns [7,11], beams [8,12], columns [13,14], beam-columns [1,2,15,16,17] and tubular joints [18,19].

In current codes of practice [20-22], the existing design rules are extended for steels with nominal yield stresses up to 690 and 700 MPa. Structural members are often subjected to combined compression and bending (i.e. beam-column). However, the existing beam-columns design rules are derived from the investigation carried out on beam-column members made of normal strength steel. Therefore, it is essential to assess the appropriateness of current design rules for CST beam-columns made of steel grades higher than or equal to S700. Usami and Fukumoto [15] and Yu and Tall [16] conducted the early investigation on built-up box- and I-section beam-columns made of HT80 (equivalent to S690) and A514 (equivalent to S690) steels, and concluded that the strengths of built-up HSS beam-columns were greater than those made of normal strength steel. Liew et al. [17] investigated the structural performance of concrete filled steel tubular beam-columns, where the

compressive strengths of concrete mixes ranged from 52 to 193 MPa, and yield stresses of steels ranged from 300 to 779 MPa. New reduction factors were proposed in Ref. [17] for the design of investigated beam-columns. The literature review confirmed that the research on CST beam-columns with steel grades higher than or equal to S700 is quite scant. Therefore, Ma et al. [1,2] conducted a series of long and short beam-column (LBC and SBC) tests on square, rectangular and circular hollow sections (SHS, RHS and CHS) members made of S700 and S900 steel grades. In the test programs [1,2] and in this study, specimens with the lengths of 2800 mm and 600 mm were defined as LBC and SBC, respectively. The appropriateness of design provisions given in AISC [22], AS [23] and EC3 [24] specifications for CFHSS tubular beam-columns were assessed through the obtained test results [1,2]. The comparison of limited test results showed that the existing design provisions are conservative, and therefore, they are not economical for the design of CFHSS tubular beam-columns. Thus, it becomes essential to extend the data pool to understand the overall structural performance of CFHSS tubular beam-columns, to comprehensively check the appropriateness of current design provisions and finally to propose modified design rule, which in turn formed the basis of the investigation presented in this paper. The data pool was enlarged by performing an extensive numerical parametric study which duly covered a broad range of flat width-to-thickness ratio of SHS and RHS. A modified design method has been proposed for the design of cold-formed steel SHS and RHS beam-columns made of steel grades ranged from S700 to S1100 using the tests [1,2] and numerical results obtained in this study.

2. Summary of experimental investigation

Tests were carried out by Ma et al. [1,2] to examine the structural performance of CFHSS SHS, RHS and CHS long and short beam-columns. In total, 32 LBC and 51 SBC specimens were tested. The nominal steel grades of LBC and SBC test specimens were S700 and S900. The mechanical properties of tubular members used in tests [1,2] are detailed in Table 1, where E, $\sigma_{0.2}$, σ_u and ε_{25mm} denote initial Young's modulus, 0.2% proof stress, ultimate stress and fracture strain. For LBC tests, 1 SHS (H80×80×4), 1 RHS (H100×50×4) and 1 CHS (V89×3) members were investigated. On the other hand, for SBC tests, 5 SHS (H80×80×4, H120×120×4, H140×140×6, V80×80×4, V120×120×4)

and 2 RHS (H100×50×4 and H200×120×5) were investigated. All test specimens had pinned end boundary conditions and were subjected to concentric and eccentric compression loads. RHS beam-columns were tested along both major and minor axes. The test specimens reported in Ma et al. [1,2] were grouped in accordance with the cross-section dimensions. Within each group, one test specimen was loaded concentrically to obtain pure compression capacity of the column, and for the remaining test specimens of a group, axial compression loads (P) were applied with different initial loading eccentricities. The lengths of all LBC test specimens were 1480 mm, while the lengths of SBC test specimens were designed in accordance with the cross-section dimensions of tubular members. In the labelling of the test specimen, the first letter denotes the series, where test specimens with nominal steel grades of S700 and S900 were denoted by H and V series, respectively, followed by width (B), depth (H) and thickness (t) of the cross-section. In order to keep the labelling of beam-column specimen different to those of beam and column specimens, the term BC (i.e. beam-column) was added to the label. Finally, the nominal value of initial loading eccentricity (e) was then suffixed to the overall label. If a test is repeated, the letter 'R' was then added at the end of the overall label.

Global and local geometric imperfections were measured and considered in the analyses of LBC and SBC test specimens, respectively. For SHS and RHS long beam-column test specimens, the mean absolute values of measured global geometric imperfections at the mid-lengths of different groups of test specimens ranged from L/4107 to L/3479, where L is the specimen length. For SBC test specimens, the maximum value of local geometric imperfection was denoted by δ, while the flat width-to-thickness ratio was denoted by α, where $\alpha = (B\text{-}2R_0)/t$ or $(H\text{-}2R_0)/t$. The term R_0 represents external corner radius of SHS and RHS. For the H series test specimens, the mean value of δ/α ratio was 0.0119, while it was 0.0146 for the V series test specimens. Both LBC and SBC specimens were tested in servo-controlled hydraulic testing machines using displacement-control loading, as shown in Fig. 1. The axial shortening and rotation at the loading end were measured using three pre-calibrated linear variable displacement transducers (LVDTs). Moreover, lateral deflection at the mid-length (δ_y) due to bending of LBC and SBC test specimens was measured using two LVDTs. In addition, at the mid-length of the test specimen, four strain gauges were attached near the end of the flat regions in the bending plane, as shown in Fig. 2. The test specimens were adjusted along the slot

holes machined on both wedge plates to achieve different initial loading eccentricities. For all LBC and SBC test specimens, the test curves were converted into static curves using the load drops obtained by pausing the test machine. The test results were obtained from the static curves, where the influence of strain rate was absent.

All LBC test specimens failed by global buckling and showed significant second-order effects under applied axial compression loads. As the cross-sections of LBC test specimens were compact, therefore no local buckling was noticed during the tests. On the other hand, section yielding and local buckling were generally the dominant failure modes for SBC test specimens. The influence of second-order effects and global geometric imperfections were found negligible in all SBC test specimens. Moreover, the influence of local geometric imperfections was found negligible in all LBC test specimens. The flexural behaviour of tubular members used in Ma et al. [1,2] was investigated by Ma et al. [8] using four-point bending tests, and the obtained ultimate moment capacities (M_u) are detailed in Table 2. The test results, including ultimate compression capacities (P_u) and corresponding end moments ($M_{end,u}$), mid-length moments ($M_{mid,u}$) and end rotations (θ), are reported in Ma et al. [1,2]. The nominal strengths calculated from AISC [22], AS [23] and EC3 [24] specifications were then evaluated against the ultimate compression capacities of test specimens. It has been demonstrated that these specifications [22-24] underestimated the ultimate capacities of CFHSS long and short beam-columns by 3% – 14% and 13% – 21%, respectively. The experimental programs of CFHSS long and short beam-columns are detailed in Ma et al. [1,2].

3. Numerical investigation

3.1. General

The details of the numerical program conducted on CFHSS SHS and RHS beam-columns are presented in this section. The numerical investigation was performed using ABAQUS [25]. The finite element (FE) models were developed using measured material properties, member dimensions and eccentricities. In addition, measured initial global and local geometric imperfections were also included in the FE models. Moreover, the influences of cold-working and residual stress are also discussed in the following sub-sections of this paper.

144

145 3.2. Type of element and material modelling

146 A shell element with four nodes and double curvature along with reduced integration feature
147 (i.e., S4R) has been proved accurate and efficient to simulate various metallic materials and cross-
148 sections subjected to different loading cases [26-29]. Therefore, in this study, SHS and RHS long and
149 short beam-columns were modelled using S4R element. A mesh sensitivity analysis was conducted,
150 and finally, seedings at a spacing of (B+H)/30 along the longitudinal and transverse direction of the
151 specimen were found accurate enough for the precise replication of the test results [1,2]. In the corner
152 regions of tubular members, a relatively fine mesh was used to exactly model the corner curvatures.
153 Ma et al. [3] developed stress-strain model for the flat and corner regions of S700 and S900 steel
154 grades SHS and RHS members, which was adopted in this investigation for material modelling. In
155 order to define a material, a multi-linear stress-strain curve can be used in ABAQUS [25]. The elastic
156 region of the material definition linearly extends up to the proportional limit stress. The slope of the
157 linear part is equal to the initial Young's modulus of the material. On the other hand, in the plastic
158 region, ABAQUS [25] recommends the conversion of engineering stress-strain curve into a true
159 stress (σ_{true}) and logarithmic plastic strain ($\varepsilon_{true,pl}$) curve using Eqs. (1) and (2).

$$\sigma_{true} = \sigma\left(1+\varepsilon\right) \tag{1}$$

$$\varepsilon_{true,pl} = \ln\left(1+\varepsilon\right) - \sigma_{true} / E \tag{2}$$

160 In Eqs. (1) and (2), σ and ε respectively represent the stress and strain values obtained from the
161 measured static stress-strain curve. By following this approach, material definitions were developed
162 for the flat and corner portions of SHS and RHS members, and subsequently, they were assigned to
163 their corresponding regions in the FE models.

164 During the cold-working process, bending and membrane residual stresses are introduced in
165 the cold-formed sections. The pattern and magnitude of these residual stresses were comprehensively
166 investigated by Ma et al. [3] along both longitudinal and transverse directions of CFHSS tubular
167 members. Ma et al. [3] reported significant presence of bending residual stresses along the
168 longitudinal direction of CFHSS tubular members. On the contrary, membrane residual stresses were
169 present in small amounts along both longitudinal and transverse directions of CFHSS tubular

members. The bending stresses released during the cutting of coupon specimens from tubular members were restored during the tensile tests of coupon specimens [30]. Therefore, the constitutive material model developed by Ma et al. [3] had implicitly included the effects of bending residual stresses. On the other hand, it has been concluded in many studies [31-33] that membrane residual stresses have trivial effects on the overall structural behaviour of different cold-formed metallic members and subjected to various loadings. The maximum values of measured longitudinal membrane residual stresses reported by Ma et al. [3] were less than 20% of the yield stresses of investigated CFHSS tubular members, and their effects were negligible on the accuracies of FE models [7,8]. Therefore, in order to keep the modelling methodology simple, in this study, the explicit inclusion of residual stresses was ignored in the FE models of CFHSS long and short beam-columns. Compared to the flat portions of CFHSS tubular members, the corner portions exhibit relatively enhanced strength due to significant amount of cold-working in HSS sections. Therefore, it is essential to consider the strength enhancements of corner portions of SHS and RHS in the FE models. The variations of material strength along the cross-section of CFHSS SHS and RHS was studied by Ma et al. [3]. The findings of this investigation [3] proved that the strengths of flat regions adjacent to the corner regions also increased. Hence, in this investigation, the influence of cold-working was included in FE models by assigning wider corner regions. Thus, for the validation of test results, actual corner regions were extended by t, $2t$ and $3t$ distances into the adjacent flat regions, as shown in Fig. 3. Finally, corner regions were extended up to $2t$ into the adjacent flat regions to include the influence of cold-working in HSS sections, which is in agreement with several other studies conducted on CFHSS tubular members and joints [7,8,34,35].

3.3. Boundary condition and load application

As detailed in Ma et al. [1,2], both LBC and SBC specimens were tested under concentric and eccentric compression loads. The pinned end boundary condition of beam-column was achieved using a parallel sharp pointed edge between wedge and pit plates, as shown in Fig. 4. Therefore, in order to numerically simulate the boundary conditions of beam-columns with zero nominal eccentricity (i.e. e=0), a reference point was kinematically coupled to the surface of each end cross-

198 section. The effective length (L_e) of beam-column specimen is shown in Fig. 4 and is equal to the
199 length of specimen (L) and total heights of wedge and end plates at both ends. For both LBC and
200 SBC test specimens, the total height of pin, wedge plate and end plate was 87.5 mm, therefore,
201 reference points were positioned at 87.5 mm from the cross-section end. For eccentrically loaded
202 beam-column specimens, these two reference points were then laterally offset in the bending plane
203 by a distance equal to the measured loading eccentricity. In order to exactly reciprocate experimental
204 boundary conditions, both top and bottom reference points were allowed to rotate in the bending
205 plane, and the bottom reference point was also allowed to translate along the length of the specimen.
206 All other degrees of freedom (DOF) of the top and bottom reference points were restrained. Moreover,
207 the DOF of all nodes of LBC and SBC specimens were kept unrestrained. Using displacement control
208 load, axial compression was then applied at the bottom reference point of the specimen by duly
209 following the static RIKS procedure given in ABAQUS [25]. The parameter that enables the FE
210 model to undergo large non-linear deformation (*NLGEOM) was activated during the FE analysis.
211 In addition, the size of step increment was kept small in the RIKS procedure in order to obtain smooth
212 load-deflection and load-end rotation curves.
213
214 3.4. Modelling of initial geometric imperfections
215 The measured global and local geometric imperfections were incorporated in the FE models of
216 LBC and SBC specimens, respectively. The global and local geometric imperfection profiles were
217 obtained by conducting elastic buckling analyses on identical FE specimens. The BUCKLE
218 command of ABAQUS [25] was used to implement this methodology. Through elastic buckling
219 analysis, which is also termed as eigenvalue analysis, the global and local buckling imperfection
220 profiles were separately obtained for LBC and SBC specimens, respectively. The first mode of elastic
221 buckling analysis of FE specimen was treated as the imperfection mode of that specimen. The
222 deformation scale of the first buckling mode was then ramped up to the measured values of geometric
223 imperfections. The scaled eigenmode shape was then superimposed on the beam-column FE model.
224 The effect of local geometric imperfection was negligible on the ultimate capacities of LBC
225 specimens [1]. On the other hand, the effect of global geometric imperfection was negligible on the

ultimate capacities of SBC specimens [2]. The approach adopted in this study for the inclusion of initial geometric imperfection was consistent with the approach adopted in other similar investigation on beam-columns [31-33]. The measured values of geometric imperfection used in the verification of LBC and SBC FE specimens are reported in Ma et al. [1,7].

3.5. Validation of finite element models

The modelling methodologies explained in the previous sections of this paper were used by Ma et al. [1,2] to develop and calibrate FE models for CFHSS long and short beam-columns. The LBC and SBC finite element models were validated using 24 LBC tests [1] and 51 SBC tests [2], respectively. For validation, the ultimate capacities of LBC and SBC test specimens ($P_{Exp,LBC}$, $P_{Exp,SBC}$) were compared with those predicted from their corresponding FE models ($P_{FE,LBC}$, $P_{FE,SBC}$). During the validation process, failure modes, load-deflection and load-end rotation curves were also compared between all test and FE specimens. Table 3 presents the comparisons of the ultimate compression capacities of LBC test specimens ($P_{Exp,LBC}$) with the compression capacities predicted from corresponding FE models ($P_{FE,LBC}$). The values of mean and coefficients of variation (COV) of this comparison are 0.98 and 0.024, respectively. Moreover, Fig. 5 presents the comparisons of load-deflection curves between test and FE model for H80×80×4 long beam-columns. In addition, Fig. 6 presents the comparisons of failure mode between test and FE model for H80×80×4-BC-e40 long beam-column. From Table 3 and Figs. 5 and 6, it is evident that the ultimate compression capacities, load-deflection curves and failure mode of LBC specimens were closely predicted by the validated LBC FE model.

For SBC specimens, the comparisons of ultimate compression capacities between tests ($P_{Exp,SBC}$) and FE ($P_{FE,SBC}$) models are shown in Table 4. The accuracy of the SBC FE model was verified using 51 SBC tests conducted by Ma et al. [2]. From Table 4, it can be noted that the mean value of test-to-FE ratios of ultimate capacities is 0.98 and the corresponding COV is 0.042. On the other hand, the comparisons of load-end rotation curves between test and FE model of H120×120×4 short beam-columns are shown in Fig. 7. Furthermore, Fig. 8 presents the comparisons of failure mode between test and FE model for short beam-columns. From these comparisons, it is apparent that the validated

SBC FE model accurately replicated the overall structural behaviour of S700 and S900 steel grades SHS and RHS short beam-columns.

3.6. Parametric study

This section discusses the parametric study conducted on CFHSS long and short beam-columns. The parametric study was conducted with an aim to enlarge the data pool by duly including a broad range of cross-section dimensions and member slenderness. In total, 390 specimens, including 195 LBC and 195 SBC specimens, were analysed in the parametric study. The FE specimens having nominal yield stress of 700 MPa, 900 MPa and 1100 MPa were denoted by H, V and S series, respectively. Each series of both LBC and SBC specimens include 5 SHS and 8 RHS sections, wherein for each section, axial compression was applied with one concentric and four eccentric loadings. The FE methodologies used to validate long and short beam-column FE models were also adopted in their corresponding parametric studies. The constitutive stress-strain model developed by Ma et al. [3] was assigned to the flat and extended corner regions of CFHSS long and short beam-column specimens. The cross-section dimensions of SHS and RHS beam-column specimens varied from 40 mm to 300 mm, while the values of flat width-to-thickness ratio varied from 7.5 to 96. The lengths of all LBC and SBC specimens were kept equal to 2800 mm and 600 mm, respectively, in the parametric study. The corner regions of all FE specimens were extended into the adjacent flat regions by 2t. The value of global geometric imperfection adopted in the FE models of LBC was L/1500. On the other hand, the value of local geometric imperfection adopted in the FE models of SBC was in accordance with the recommendations proposed by Ma et al. [7]. The total length of all FE models was equal to the sum of the lengths of specimens (L) and total heights of end and wedge plates at each end of the specimens (87.5 mm), i.e., $L_e = L + 2\times87.5$ mm.

The ultimate compression capacities of SHS and RHS long beam-column specimens obtained from tests [1] and numerical investigation conducted in this study are detailed in Table 5. On the other hand, Table 6 presents the ultimate compression capacities of SHS and RHS short beam-column specimens obtained from tests [2] and the parametric study. The FE specimens of the parametric study were labelled as "series, B, H, t, *LBC* or *SBC*, e". In the labelling, series represent for H, V and S series; followed by cross-section width (B), depth (H) and thickness (t) of the tubular member; *LBC* and *SBC* stand for long and short beam-columns, respectively; and e stands for the nominal value of initial loading eccentricity. In this investigation, the values of initial loading eccentricity of LBC and

SBC specimens ranged from $H/40$ to H. In the parametric study, short beam-columns with large member slenderness were generally failed by global buckling, while remaining short beam-columns were generally failed by either local buckling or section yielding. On the other hand, global buckling was the dominant failure mode for long beam-columns with compact cross-sections, while the long beam-columns with large values of flat width-to-thickness ratio were failed by interaction of global and local buckling.

4. Existing design provisions

4.1. Background

Although the design rules given in the latest editions of AISC [22], AS [20] and EC3 [21] permit the use of steels with nominal steel grades up to S690 and S700, however, it should be noted that the current design provisions given in the specifications [22-24] are mainly developed from the research conducted on specimens made of normal strength steel. Therefore, it becomes essential to examine the appropriateness of current design rules given in AISC [22], AS [23] and EC3 [24] for CFHSS tubular beam-columns. The following sub-sections briefly detailed the beam-column design rules given in these specifications [22-24].

4.2. AISC [22]

A two-phase interactive relationship is given in AISC [22], as shown in Eq. (3), to design a doubly or singly symmetric member undergoing concurrent axial load and bending. In Eq. (3), the ratio of ultimate compression load (P_u) normalised with nominal predicted pure compression capacity (P_n) is linearly proportioned to the ratio of second-order bending moment (M_u) normalised with nominal predicted pure bending capacity (M_n). For members subject to uniaxial bending and possess single uniform curvature along their length, M_u can be determined by amplifying the end moment ($M_{end,u}$), as shown in Eq. (4). The term P is the applied load, and P_{cr} is the Euler's critical buckling load in Eq. (4).

$$\begin{cases} \dfrac{P_u}{P_n} + \dfrac{8}{9}\dfrac{M_u}{M_n} \le 1 \quad \text{for} \quad \dfrac{P_u}{P_n} \ge 0.2 \\ \dfrac{P_u}{2P_n} + \dfrac{M_u}{M_n} \le 1 \quad \text{for} \quad \dfrac{P_u}{P_n} < 0.2 \end{cases} \tag{3}$$

$$M_u = \frac{M_{end,u}}{(1 - P/P_{cr})} \tag{4}$$

311

312 4.3. AS [23]

313 The interactive relationship given in AS [23] to design a beam-column member is shown in Eq.
314 (5). A more simplified version of Eq. (5) is shown in Eq. (6). Similar to the design rule given in AISC
315 [22], the ratio of ultimate compression load (P_u) normalised with nominal predicted pure compression
316 capacity (P_n) is linearly proportioned to the ratio of second-order bending moment (M_u) normalised
317 with nominal predicted pure bending capacity (M_n). The second-order bending moment (M_u) can be
318 calculated using the amplification factor detailed in Section 4.2 of this paper for AISC [22], and
319 shown in Eq. (4). Moreover, as the cold-formed sections used in tests [1,2] were non-stress relieved,
320 therefore, a compression member section constant (α_b) equal to -0.50 was adopted to calculate the
321 nominal pure compression capacity (P_n) of beam-column specimen.

$$M_u \le M_n\left(1 - \frac{P_u}{P_n}\right) \tag{5}$$

$$\frac{P_u}{P_n} + \frac{M_u}{M_n} \le 1 \tag{6}$$

322

323 4.4. EC3 [24]

324 The approach adopted in EC3 [24] for the design of a beam-column member is similar to those
325 adopted in AISC [22] and AS [23] specifications. However, unlike the linear interaction formulae
326 given in AISC [22] and AS [23], the design rule given in EC3 [24] uses an interaction factor (k_{yy}) to
327 consider the non-linear beam-column interaction relationship, as shown in Eq. (7). Unlike the use of
328 second-order design moment in the beam-column design rules given in AISC [22] and AS [23]
329 specifications, the first-order design moment is used in the interaction formula given in Eq. (7) [36].
330 Therefore, $M_{end,u}$ has been used in Eq. (7) instead of M_u. The calculation of interaction factor (k_{yy})

has been demonstrated through two methods in EC3 [24] specification. The method-1 given in the Annex-A of EC3 [24] is more accurate, and therefore, it was used in this study to calculate k_{yy}. Furthermore, buckling curve 'c' given in EC3 [24] and recommended for cold-formed hollow sections was used to calculate nominal capacities under pure compression (P_n).

$$\frac{P_{\mathrm{u}}}{P_{\mathrm{n}}}+k_{\mathrm{yy}}\frac{M_{\mathrm{end,u}}}{M_{\mathrm{n}}}\leq 1 \tag{7}$$

5. Reliability analysis

In order to ensure that the current and proposed design rules are reliable, a reliability analysis was conducted as per AISI [37]. The target reliability index (β_0), as shown in Eq. (8), was calculated in accordance with Section K2.1.1 of AISI [37]. In this investigation, a lower bound limit of 2.50 was used as the value of the target reliability index (β_0). Therefore, when the value of target reliability index (β_0) calculated using Eq. (8) was greater than or equal to 2.50, the design rule was treated as reliable in this study. The reliability index (β_0) is related to other associated governing parameters as follows:

$$\beta_0=\frac{\ln(C_\phi M_m F_m P_m/\phi)}{\sqrt{V_M^2+V_F^2+C_P V_P^2+V_Q^2}} \tag{8}$$

In Eq. (8), the calibration coefficient (C_ϕ) was calculated using a dead load (DL)-to-live load (LL) ratio of 0.20. For the material factor, the mean value and COV were denoted by M_m and V_M, respectively. On the other hand, for the fabrication factor, the mean value and COV were denoted by F_m and V_F, respectively. The resistance factor required to convert nominal strength to design strength was denoted by ϕ. The mean value of ratios of test and FE strengths of specimen-to-nominal strengths predicted from code was denoted by P_m, while the corresponding COV was denoted by V_P. In order to account for the effect of data size, a correction factor (C_P) recommended in AISI [37] was also used in Eq. (8). Besides, the COV of the load effects was represented by V_Q. In Eq. (8), the values of mean (M_m) and COV (V_M) of the material factor were taken as 1.1 and 0.10, respectively. Additionally, in the calculation of β_0, the values of mean (F_m) and COV (V_F) of the fabrication factor were taken as 1.0 and 0.05, respectively. The values of mean (P_m) and COV (V_P) of comparisons

between test and FE strengths with nominal predicted strengths can be obtained from Tables 5-7. For the purpose of evaluating the appropriateness of the design rule given in AISC [22], the load combination was taken as 1.2DL + 1.6LL, while the values of the calibration coefficient (C_ϕ) and resistance factor (ϕ) were taken as 1.521 and 0.90, respectively. Further, to examine the suitability of the design rule given in AS [23], the load combination was taken as 1.2DL + 1.5LL, while the values of calibration coefficient (C_ϕ) and resistance factor (ϕ) were taken as 1.445 and 0.90, respectively. In order to assess the adequacy of the design rule given in EC3 [24] for CFHSS tubular beam-columns, the load combination was taken as 1.35DL + 1.5LL, while the values of calibration coefficient (C_ϕ) and resistance factor (ϕ) were taken as 1.463 and 1.0, respectively.

6. Comparison of nominal predicted capacities with beam-column capacities

The comparisons of ultimate compression capacities obtained from tests [1,2] and FE analyses conducted in this study with nominal capacities predicted from AISC [22], AS [23] and EC3 [24] are discussed in this section of the paper. A total of 465 data was used for the comparison, including 24 LBC test strengths [1], 51 SBC test strengths [2], 195 LBC numerical strengths and 195 SBC numerical strengths. In order to predict the strengths from the interaction curves of AISC [22], AS [23] and EC3 [24] specifications, the data points on the load-moment interaction curves of these specifications [22-24] were determined using a line intersecting these curves with slope equal to the initial loading eccentricity (e) of the specimen, as shown in Fig. 9. The terms P_y and M_p respectively represent yield load and plastic moment of the cross-section of tubular member in Fig. 9. Tables 5 and 6 present the comparisons of test and FE strengths-to-predicted strengths for CFHSS beam-columns. The comparisons are also graphically shown in Figs. 10-12. Furthermore, the overall summary of the comparison results is detailed in Table 7.

The comparisons of experimental and numerical ultimate compression capacities (P_u) of CFHSS long and short beam-columns with the nominal capacities predicted from AISC [22] (P_{AISC}) are presented in Tables 5-7 and Fig. 10. For LBC specimens, the values of mean and COV of experimental and numerical capacities (P_u)-to-nominal capacities from AISC [22] (P_{AISC}) are 1.01 and 0.114, respectively. On the other hand, for SBC specimens, the values of mean and COV of

experimental and numerical capacities (P_u)-to-nominal capacities from AISC [22] (P_{AISC}) are 1.07 and 0.092, respectively. For the overall comparison, including LBC and SBC specimens, the values of mean and COV of experimental and numerical capacities (P_u)-to-nominal capacities from AISC [22] (P_{AISC}) are 1.04 and 0.106, respectively. In AISC [22], the values of resistance factors recommended for both axial compression (ϕ_c) and bending (ϕ_b) are equal to 0.90. Thus, the value of β_0 calculated using Eq. (8) is 2.53. Therefore, in general, it is evident from the comparisons that the ultimate compression capacities of S700, S900 and S1100 steel grades cold-formed SHS and RHS long and short beam-columns are accurately and reliably predicted by the design rule given in AISC [22].

The comparisons of experimental and numerical ultimate compression capacities (P_u) of CFHSS long and short beam-columns with the nominal capacities predicted from AS [23] (P_{AS}) are presented in Tables 5-7 and Fig. 11. For LBC specimens, the values of mean and COV of experimental and numerical capacities (P_u)-to-nominal capacities from AS [23] (P_{AS}) are 1.10 and 0.068, respectively. On the other hand, for SBC specimens, the values of mean and COV of experimental and numerical capacities (P_u)-to-nominal capacities from AS [23] (P_{AS}) are 1.19 and 0.068, respectively. For the overall comparison, including LBC and SBC specimens, the values of mean and COV of experimental and numerical capacities (P_u)-to-nominal capacities from AS [23] (P_{AS}) are 1.15 and 0.077, respectively. The values of resistance factors for both axial compression (ϕ_c) and bending (ϕ_b) are equal to 0.90 in AS [23]. Thus, the value of β_0 calculated using Eq. (8) is 2.81. From the overall comparisons that include both LBC and SBC specimens, it can be noticed that AS [23] standard provides the most conservative predictions for the ultimate capacities of S700, S900 and S1100 steel grades cold-formed SHS and RHS long and short beam-columns.

Tables 5-7 and Fig. 12 present the comparisons of experimental and numerical ultimate capacities (P_u) of CFHSS long and short beam-columns with the nominal capacities predicted from EC3 [24] (P_{EC3}). For LBC specimens, the values of mean and COV of experimental and numerical capacities (P_u)-to-nominal capacities from EC3 [24] (P_{EC3}) are 1.11 and 0.088, respectively. On the other hand, for SBC specimens, the values of mean and COV of experimental and numerical capacities (P_u)-to-nominal capacities from EC3 [24] (P_{EC3}) are 1.16 and 0.086, respectively. For the

411 overall comparison, including LBC and SBC specimens, the values of mean and COV of
412 experimental and numerical capacities (P_u)-to-nominal capacities from EC3 [24] (P_{EC3}) are 1.13 and
413 0.090, respectively. The recommended value of resistance factor for members subject to compression
414 and bending is 1.0 in EC3 [24]. Thus, the value of β_0 calculated using Eq. (8) is 2.36. It is evident
415 from the overall comparison that the design method given in EC3 [24] underestimated the ultimate
416 capacities of S700, S900 and S1100 steel grades cold-formed SHS and RHS long and short beam-
417 columns by 13%. In addition, the beam-column design method given in EC3 [24] is not reliable for
418 ϕ=1.0.
419

420 **7. Proposed design method**

421 The previous section of this paper proved that the design rules given in AISC [22], AS [23] and
422 EC3 [24] specifications provide conservative predictions for the design of CFHSS tubular beam-
423 columns, particularly AS [23] and EC3 [24] specifications. The primary reason behind such
424 observation is due to significant underestimation of the end points of load-moment interaction curves
425 (i.e. pure compression strength and pure flexure strength) of CFHSS members, as illustrated in Figs.
426 13 and 14, respectively for sample LBC and SBC specimens. Similar observations were also noticed
427 for other LBC and SBC test and FE specimens.

428 EC3 [24] recommends the use of buckling curve 'c' to determine the axial compression
429 capacities of CST members, which generally underestimates the prediction capacities of
430 concentrically loaded columns by more than 20% [38]. Therefore, in this study, the buckling curve
431 'a' was used in the proposed design method. With regard to the flexural capacities of CFHSS
432 members, Ma et al. [8] investigated the pure bending capacities of CFHSS tubular beams with steel
433 grades ranged from S700 to S1100. It has been shown in Ma et al. [8] that AISC [22], AS [23] and
434 EC3 [24] specifications underestimated the flexural capacities of CFHSS SHS and RHS beams,
435 particularly for compact sections. Therefore, Ma et al. [8] proposed modified direct strength method
436 (M_{DSM}*) for the design of CFHSS tubular beams with steel grades higher than or equal to S700.
437 Schafer and Peköz [39] originally developed the direct strength method (DSM) for the design of cold-
438 formed steel open section members. The time taking effective width calculations are no longer

439 required in the DSM, which proved its superior efficiency over other methods.

440 It is evident from Fig. 15 that the DSM curve underestimated the ultimate flexural capacities
441 of CFHSS tubular beams, mainly for sections with slenderness factor of local buckling (λ_ℓ) less than
442 or equal to 0.776. Hence, Ma et al. [8] proposed modified DSM curve, as shown in Eq. (9) and Fig.
443 15, where M_{nl} stands for nominal flexural strength for local buckling and M_{ne} represents nominal
444 flexural strength for yielding and global buckling. In addition, in Fig. 15, terms M_y and M_{crl} represent
445 yield moment and critical elastic local buckling moment of cross-section, respectively. The proposed
446 modified DSM curve accurately and reliably predicted the bending capacities of S700, S900 and
447 S1100 steel grades CST beams.

$$\frac{M_{nl}}{M_{ne}} = \begin{cases} 1.5 & \text{for} \quad \lambda_\ell \le 0.539 \\ \left(\frac{1}{\lambda_\ell}\right)^{0.657} & \text{for} \quad \lambda_\ell > 0.539 \end{cases} \tag{9}$$

448 Hence, it is recommended to replace M_{n} with M_{DSM}* in the interaction formula given in EC3
449 [24], as shown in Eq. (10). The term M_{DSM}* in Eq. (10) stands for the nominal flexural capacity of
450 CFHSS tubular member and calculated in accordance with Eq. (9). The nominal ultimate
451 compression capacities of CFHSS tubular beam-columns predicted using the proposed design rule
452 (Eq. (10)) is denoted by P_{pn} in this paper.

$$\frac{P_{\mathrm{u}}}{P_{\mathrm{n}}} + k_{\mathrm{yy}} \frac{M_{\mathrm{end,u}}}{M_{\mathrm{DSM}^*}} \le 1 \tag{10}$$

453 Tables 5-6 and Fig. 16 present the comparison of test and numerical ultimate capacities with nominal
454 capacities predicted from the proposed design rule. For LBC specimens, the values of mean and COV
455 of P_u/P_{pn} are 0.99 and 0.068, respectively. On the other hand, for SBC specimens, the values of mean
456 and COV of P_u/P_{pn} are 1.06 and 0.058, respectively. For the overall comparison, including LBC and
457 SBC specimens, the values of mean and COV of P_u/P_{pn} are 1.03 and 0.072, respectively. A reliability
458 analysis was conducted using ϕ=0.85, and the value of β_0 calculated through Eq. (8) is 2.67. Fig. 16
459 demonstrated that the distribution of data is more accurate and less scattered compared to Figs. 10-
460 12. Hence, it has been demonstrated that the proposed design rule together with a resistance factor of
461 0.85, accurately and reliably predicted the ultimate compression capacities of CFHSS tubular beam-

462 columns. Moreover, the current two-phase design rule given in AISC [22] can also be used together
463 with a resistance factor of 0.90 for the design of CFHSS tubular beam-columns, however, its
464 predictions are relatively more conservative than those obtained from the proposed design rule.
465
466 **8. Conclusions**
467 The comprehensive numerical investigation and design of cold-formed high strength steel
468 (CFHSS) square and rectangular hollow sections (SHS and RHS) beam-columns are presented in this
469 paper. The numerical parametric study comprised of 390 finite element models, including 195 long
470 beam-columns models and 195 short beam-columns models. In total, three steel grades were used in
471 the parametric study, including S700, S900 and S1100. The finite element models validated by Ma
472 et al. [1,2] were employed to conduct a detailed numerical parametric study in this investigation. The
473 values of flat width-to-thickness ratio of tubular sections ranged from 7.5 to 96. In each steel grade,
474 a total of 5 SHS and 8 RHS members were investigated, where each section was subjected to one
475 concentric and four eccentric compression loads. Short beam-columns with large member
476 slenderness were generally failed by global buckling, while remaining short beam-columns were
477 generally failed by either local buckling or section yielding. On the other hand, global buckling was
478 the dominant failure mode for long beam-columns with compact cross-sections, while the long beam-
479 columns with large values of flat width-to-thickness ratio were failed by the interaction of global and
480 local buckling. The ultimate compression capacities obtained from 75 tests [1,2] and 390 numerical
481 analyses were compared with nominal capacities predicted from AISC [22], AS [23] and EC3 [24]
482 specifications. The overall comparisons demonstrated that the current design rules are conservative
483 (4% to 15%), as pure compression and pure flexural capacities of tubular members investigated in
484 this study were underestimated by AISC [22], AS [23] and EC3 [24] specifications. The current
485 design method given in EC3 [24] was improved for the design of cold-formed S700, S900 and S1100
486 steel grades tubular beam-columns by using the buckling curve ‘a’ for ultimate compression
487 capacities and the modified direct strength method proposed by Ma et al. [8] for ultimate flexural
488 capacities. The comparison results showed that the proposed design method is more accurate and
489 reliable than the beam-column design methods given in AISC [22], AS [23] and EC3 [24]

specifications. Considering the simplicity and accuracy of the proposed design method, it is suggested to use this method for the design of cold-formed steel square and rectangular hollow section beam-columns with steel grades ranged from S700 to S1100.

Acknowledgement

The work described in this paper was fully supported by a grant from the Research Grants Council of the Hong Kong Special Administrative Region, China (Project No. 17212115).

References

[1] Ma, J.L., Chan, T.M. and Young, B., 2021. Cold-formed high strength steel tubular beam-columns. Engineering Structures, 230, p.111618.

[2] Ma, J.L., Chan, T.M. and Young, B., 2019. Cold-formed high-strength steel rectangular and square hollow sections under combined compression and bending. Journal of Structural Engineering, 145(12), p.04019154.

[3] Ma, J.L., Chan, T.M. and Young, B., 2015. Material properties and residual stresses of cold-formed high strength steel hollow sections. Journal of Constructional Steel Research, 109, pp.152-165.

[4] Pandey, M. and Young, B., 2021. Stress concentration factors of cold-formed high strength steel tubular T-joints. Thin-Walled Structures, 166, p.107996.

[5] Pandey, M. and Young, B., 2021. Static resistances of cold-formed high strength steel tubular non-90° X-Joints. Engineering Structures, 239, p.112064.

[6] Zhong, Y., Sun, Y., Tan, K.H. and Zhao, O., 2021. Testing, modelling and design of high strength concrete-filled high strength steel tube (HCFHST) stub columns under combined compression and bending. Engineering Structures, 241, p.112334.

[7] Ma, J.L., Chan, T.M. and Young, B., 2018. Design of cold-formed high-strength steel tubular stub columns. Journal of Structural Engineering, 144(6), p.04018063.

[8] Ma, J.L., Chan, T.M. and Young, B., 2017. Design of cold-formed high strength steel tubular beams. Engineering Structures, 151, pp.432-443.

[9] Cai, Y. and Kwan, A.K., 2021. Behaviour and design of cold-formed austenitic stainless steel circular tubes infilled with seawater sea-sand concrete. Engineering Structures, 241, p.112435.

[10] Pandey, M. and Young, B., 2021. Post-fire mechanical response of high strength steels. Thin-Walled Structures, 164, p.107606.

[11] Gao, L., Sun, H., Jin, F. and Fan, H., 2009. Load-carrying capacity of high-strength steel box-sections I: Stub columns. Journal of Constructional Steel Research, 65(4), pp.918-924.

[12] Wang, J. and Gardner, L., 2017. Flexural buckling of hot-finished high-strength steel SHS and RHS columns. Journal of Structural Engineering, 143(6), p.04017028.

[13] Ban, H., Shi, G., Shi, Y. and Bradford, M.A., 2013. Experimental investigation of the overall buckling behaviour of 960 MPa high strength steel columns. Journal of Constructional Steel Research, 88, pp.256-266.

[14] Jiang, J., Zhang, J., Liu, J., Chiew, S.P. and Lee, C.K., 2018. Effect of welding and heat treatment on strength of high-strength steel columns. Journal of Constructional Steel Research, 151, pp.238-252.

[15] Usami, T. and Fukumoto, Y., 1982. Local and overall buckling of welded box columns. Journal of the Structural Division, 108(3), pp.525-542.

[16] Yu, C.K. and Tall, L., 1968. Welded built-up and rolled heat-treated T-1 steel columns—A514 steel beam-columns. Bethlehem, Pennsylvania: Lehigh Univ.

[17] Liew, J.R., Xiong, M. and Xiong, D., 2016, November. Design of concrete filled tubular beam-columns with high strength steel and concrete. In Structures (Vol. 8, pp. 213-226). Elsevier.

[18] Pandey, M. and Young, B., 2021. Experimental investigation on stress concentration factors of cold-formed high strength steel tubular X-joints. Engineering Structures, 243, p.112408.

[19] Pandey, M. and Young, B., 2022. Effect of member orientation on static strengths of cold-formed high strength steel tubular X-joints. Thin-Walled Structures, 170, p.108501.

[20] AS (Australian Standard). 2012. Amendment No. 1 to AS 4100-1998 steel structures. AS 4100-A1. Sydney, Australia: AS.

[21] EN 1993-1-12, Eurocode 3: Design of steel structures. Part 1-12: Additional rules for the

546 extension of EN 1993 up to steel grades S700. European Committee for Standardization (CEN),
547 Brussels, Belgium, 2007.
548 [22] ANSI/AISC 360-16 Specification for structural steel buildings. American Institude of Steel
549 Construction, Chicago, Illinois; 2016.
550 [23] AS 4100. Steel structures. Australian Standard, Sydney, Australia; 1998.
551 [24] EN 1993-1-1. Eurocode 3: Design of steel structures - Part 1–1: General rules and rules for
552 buildings. Brussels, Belgium: CEN; 2005.
553 [25] ABAQUS. ABAQUS Documentation, Dassault Syst`emes, Providence, RI, USA; 2017.
554 [26] Ren, W. X., Fang, S. E. & Young, B. (2006) Finite-element simulation and design of cold-
555 formed steel channels subjected to web crippling. Journal of Structural Engineering
556 132(12):1967-1975.
557 [27] Chan, T. M. & Gardner, L. (2008b) Compressive resistance of hot-rolled elliptical hollow
558 sections. Engineering Structures 30(2):522-532.
559 [28] Huang, Y. & Young, B. (2015) Design of cold-formed lean duplex stainless steel members in
560 combined compression and bending. Journal of Structural Engineering 141(5):04014138.
561 [29] Su, M. N., Young, B. & Gardner, L. (2014) Continuous beams of aluminum alloy tubular cross
562 sections. I: tests and FE model validation. Journal of Structural Engineering
563 10.1061/(ASCE)ST.1943-541X.0001214:04014232.
564 [30] Rasmussen, K.J.R. and Hancock, G.J., 1993. Design of cold-formed stainless steel tubular
565 members. II: Beams. Journal of Structural Engineering, 119(8), pp.2368-2386.
566 [31] Zhao, O., Gardner, L. and Young, B., 2016. Behaviour and design of stainless steel SHS and
567 RHS beam-columns. Thin-Walled Structures, 106, pp.330-345.
568 [32] Huang, Y. and Young, B., 2015. Design of cold-formed lean duplex stainless steel members in
569 combined compression and bending. Journal of Structural Engineering, 141(5), p.04014138.
570 [33] Li, Q.Y. and Young, B., 2022. Experimental and numerical investigation on cold-formed steel
571 built-up section pin-ended columns. Thin-Walled Structures, 170, p.108444.
572 [34] Pandey, M., Chung, K.F. and Young, B., 2021. Design of cold-formed high strength steel
573 tubular T-joints under compression loads. Thin-Walled Structures, 164, p.107573.
574 [35] Pandey, M., Chung, K.F. and Young, B., 2021. Numerical investigation and design of fully
575 chord supported tubular T-joints. Engineering Structures, 239, p.112063.
576 [36] Ziemian, R. D., 2010. Guide to stability design criteria for metal structures, 6th edition. John
577 Wiley & Sons.
578 [37] AISI S100, 2016. North American Specification for the Deisgn of Cold-Formed Steel Structural
579 Members, American Iron and Steel Institute.
580 [38] Ma, J., 2016. Behaviour and design of cold-formed high strength steel tubular members. HKU
581 Theses Online (HKUTO).
582 [39] Schafer, B.W., Peköz, T., 1998. Direct strength prediction of cold-formed steel members using
583 numerical elastic buckling solutions. In: 14th international specialty conference on cold-formed
584 steel structures. Rolla (MO): University of Missouri-Rolla; p. 69–76.

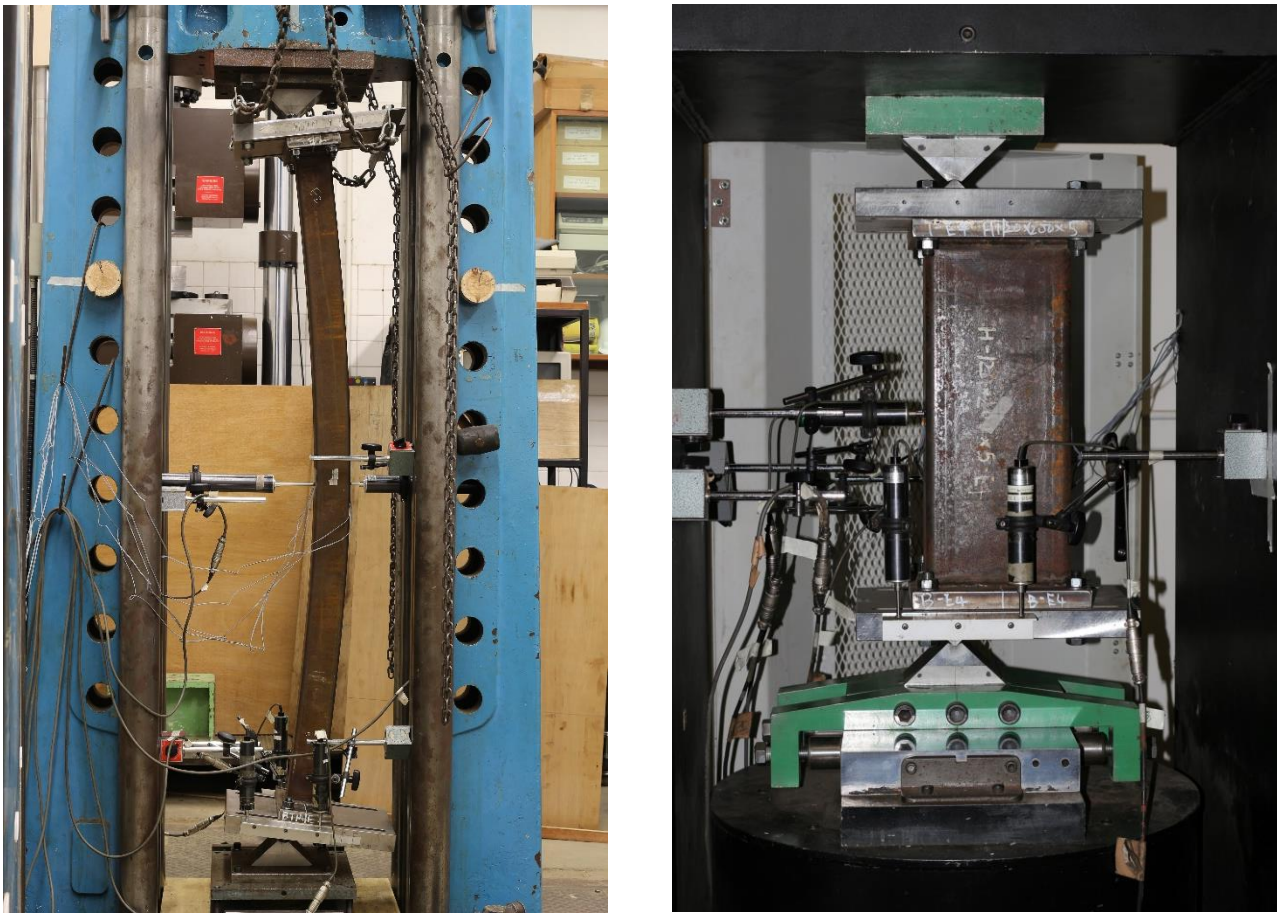

(a) Long beam-column (b) Short beam-column

Fig. 1. Test setups of long and short beam-columns

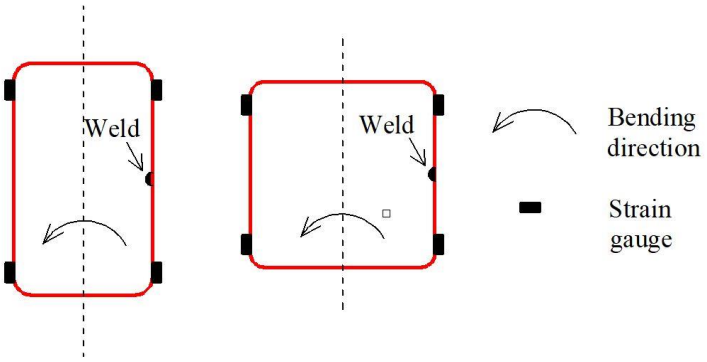

Fig. 2. Strain gauge arrangement for beam-columns

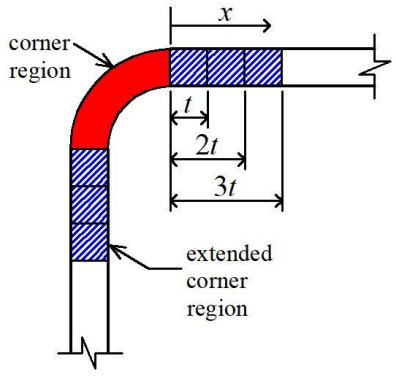

Fig. 3. Extension of corner region in finite element model

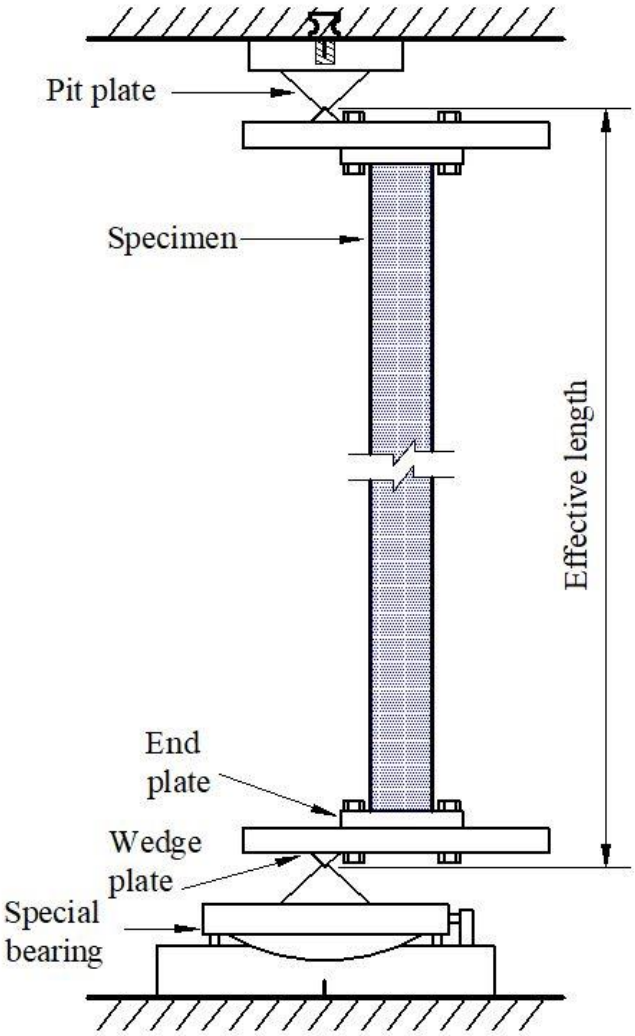

Fig. 4. Schematic sketch of beam-column test setup

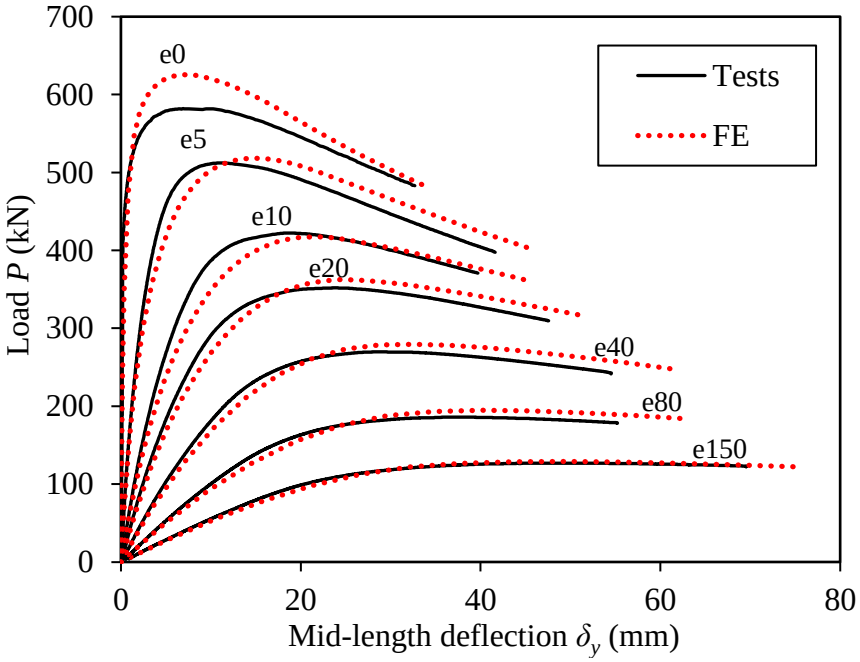

Fig. 5. Comparisons of test and FE load-deflection curves of H80×80×4 long beam-columns

Fig. 6. Comparison of test and FE global buckling failure mode for H80×80×4-BC-e40 long beam-column

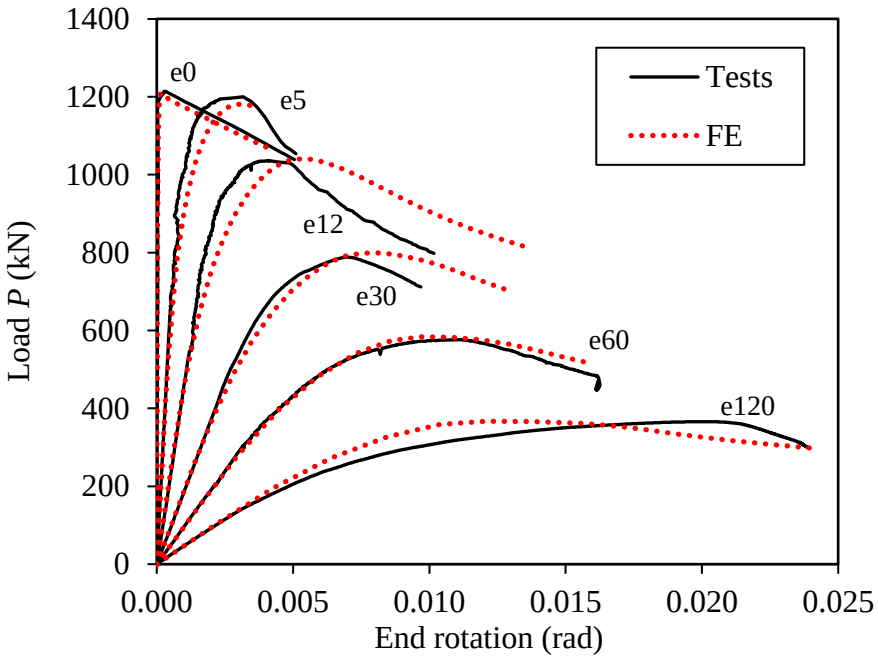

Fig. 7. Comparisons of test and FE load-end rotation curves of H120×120×4 short beam-columns

(a) Local buckling failure mode (H120×120×4-BC-e30)

(b) Section yielding failure mode (H80×80×4-BC-e80)

Fig. 8. Comparison of test and FE failure modes for short beam-columns

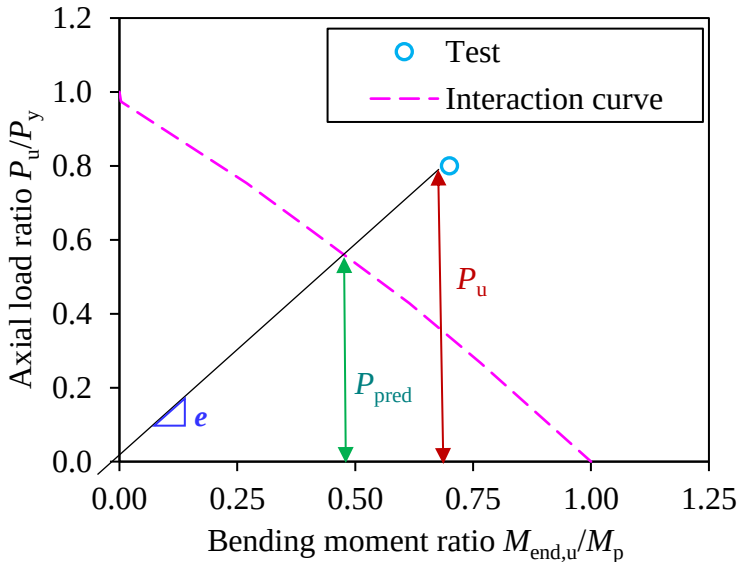

Fig. 9. Example of comparison between test and prediction from code

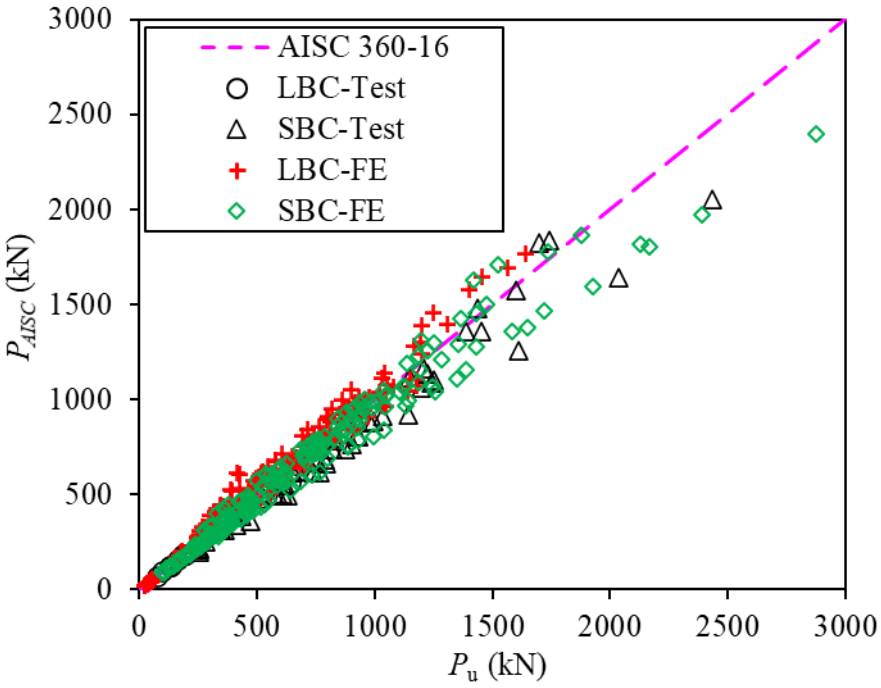

Fig. 10. Comparison of test and FE ultimate compression capacities with nominal predictions from AISC [22]

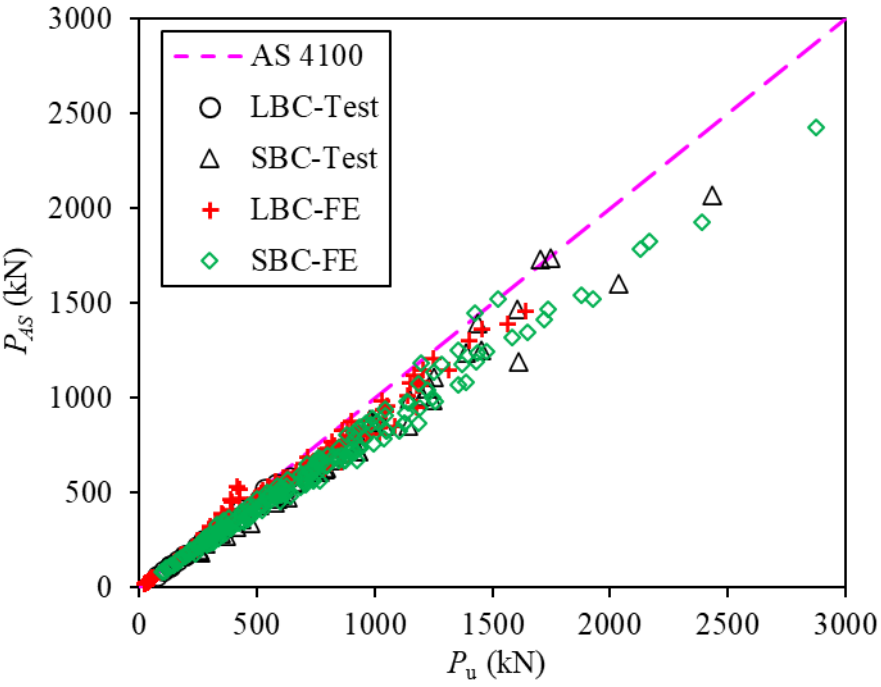

Fig. 11. Comparison of test and FE ultimate compression capacities with nominal predictions from AS [23]

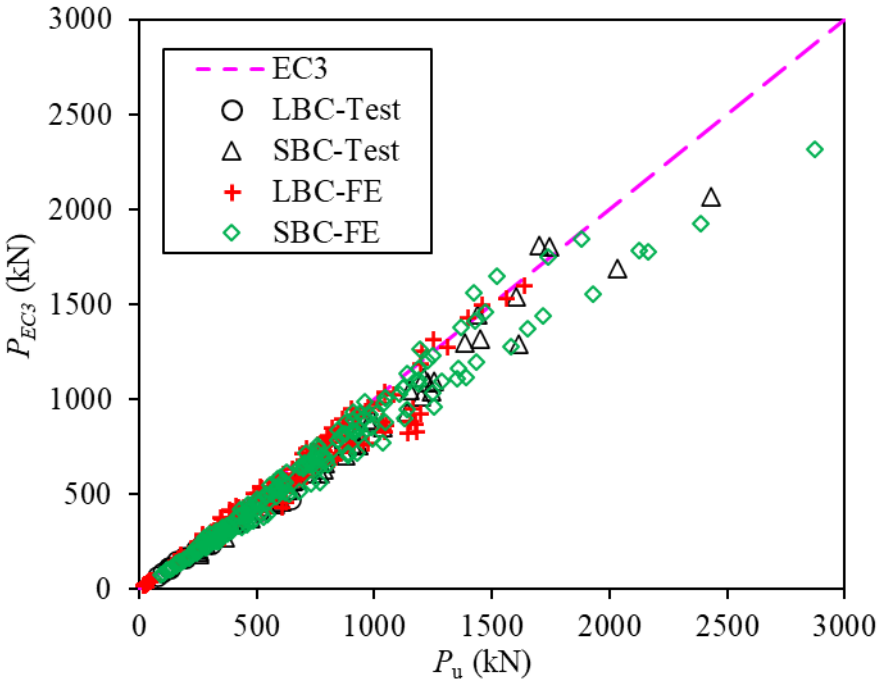

Fig. 12. Comparison of test and FE ultimate compression capacities with nominal predictions from EC3 [24]

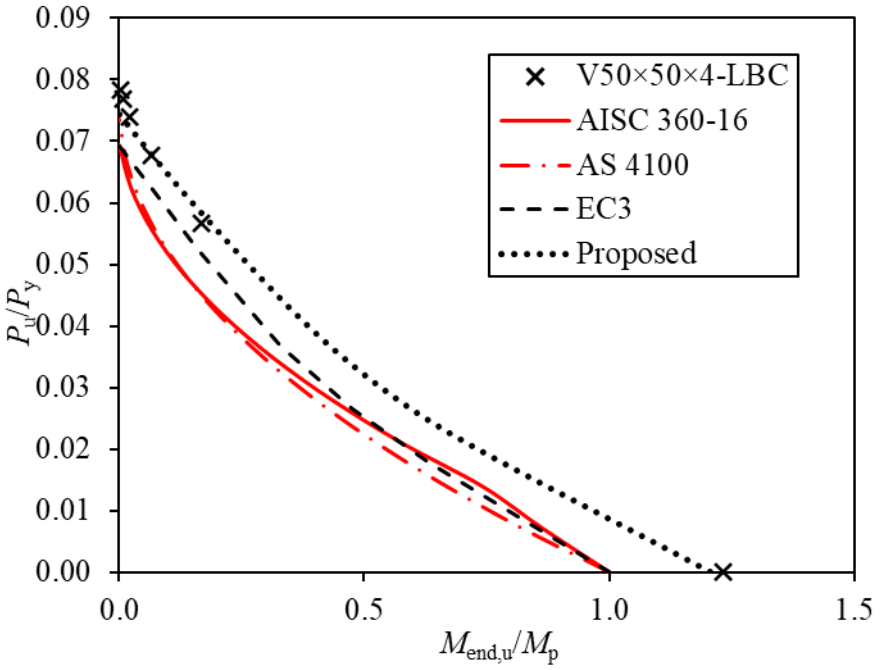

Fig. 13. Comparison of interaction curves for V50×50×4-LBC

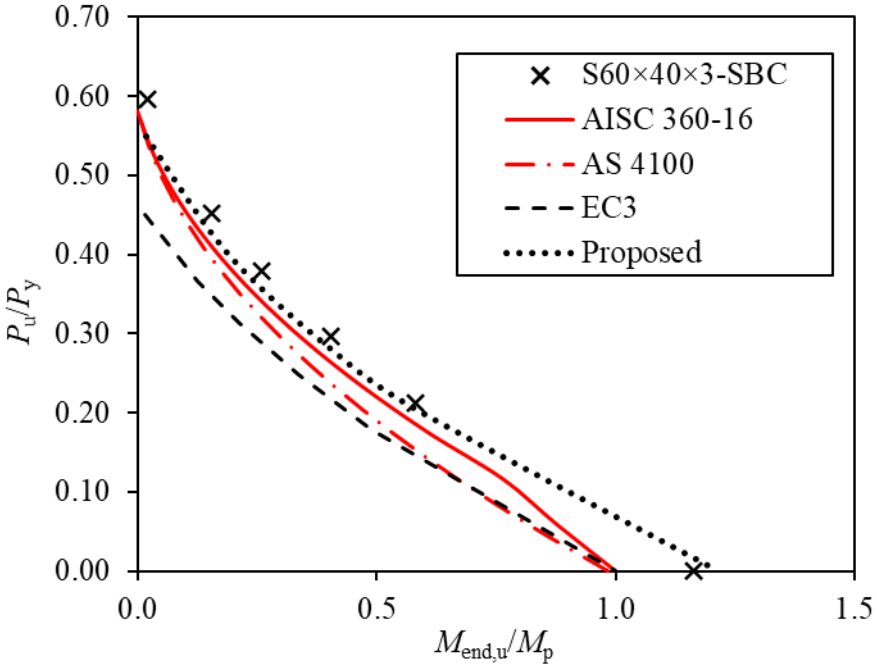

Fig. 14. Comparison of interaction curves for S60×40×3-SBC

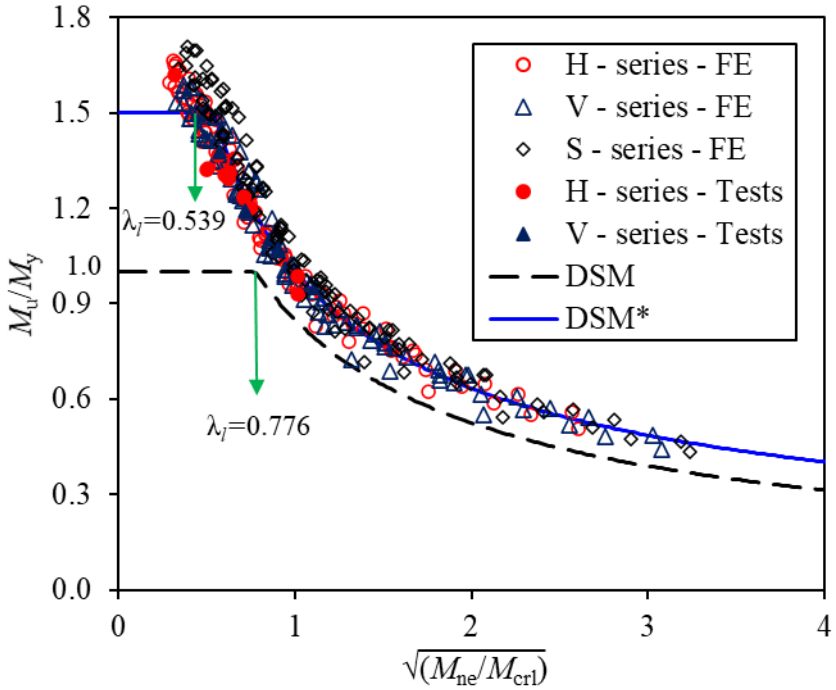

Fig. 15. Comparison of test and FE ultimate flexural capacities with original and proposed DSM curves [8]

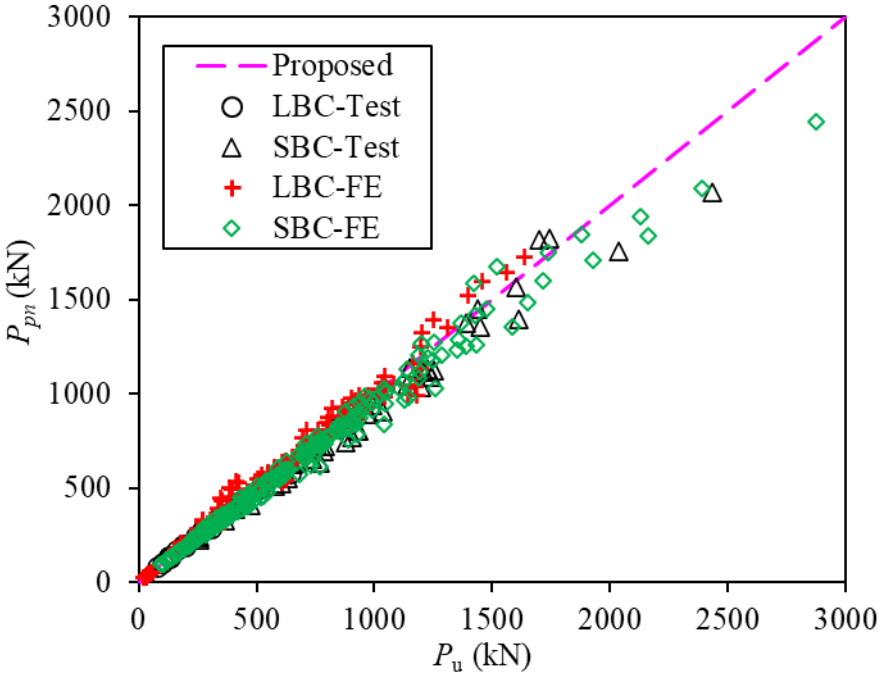

Fig. 16. Comparison of test and FE ultimate compression capacities with nominal predictions from proposed design method

Table 1 Measured flat and corner regions material properties of tubular members [3].

Section	Flat Region				Corner Region			
	E (GPa)	$\sigma_{0.2}$ (MPa)	σ_u (MPa)	ε_{25mm} (%)	E (GPa)	$\sigma_{0.2}$ (MPa)	σ_u (MPa)	ε_{25mm} (%)
H80×80×4	218	792	888	14	219	933	1005	10
H120×120×4	212	689	813	17	217	923	996	10
H140×140×6	201	663	808	18	210	859	959	11
H100×50×4	208	724	831	17	207	859	944	13
H200×120×5	207	738	846	18	205	895	970	12
V80×80×4	210	1005	1187	11	208	1187	1299	10
V120×120×4	204	960	1153	13	205	1114	1238	12

Table 2 Ultimate flexural capacities of tubular members [8].

Specimen $B\times H\times t$ (mm)	Ultimate moment capacity M_u (kNm)
H80×80×4	28.1
H120×120×4	56.1
H140×140×6	121.7
H100×50×4	16.9
H50×100×4	30.9
H200×120×5	90.3
H120×200×5	157
V80×80×4	37.5
V120×120×4	68.6

Table 3 Comparisons of Test and FE ultimate compression capacities for Long Beam-Columns [1].

Specimen	$P_{Exp,LBC}$ (kN)	$P_{FE,LBC}$ (kN)	$P_{Exp,LBC}/P_{FE,LBC}$
H50x100x4-BC-e0	642.3	631.6	1.02
H50x100x4-BC-e3	531.6	555.0	0.96
H50x100x4-BC-e10	432.7	453.2	0.95
H50x100x4-BC-e10-R	426.9	445.9	0.96
H50x100x4-BC-e20	364.8	380.8	0.96
H50x100x4-BC-e40	273.6	288.0	0.95
H50x100x4-BC-e80	195.0	198.7	0.98
H50x100x4-BC-e150	132.7	132.8	1.00
H100x50x4-BC-e0	306.9	300.6	1.02
H100x50x4-BC-e5	241.6	239.5	1.01
H100x50x4-BC-e15	193.6	194.1	1.00
H100x50x4-BC-e30	159.4	164.1	0.97
H100x50x4-BC-e50	128.4	129.4	0.99
H100x50x4-BC-e50-R	129.0	130.7	0.99
H100x50x4-BC-e80	98.7	100.9	0.98
H100x50x4-BC-e130	76.2	76.6	0.99
H80x80x4-BC-e0	581.9	625.5	0.93
H80x80x4-BC-e3	512.3	518.1	0.99
H80x80x4-BC-e10	422.2	417.5	1.01
H80x80x4-BC-e20	351.9	362.4	0.97

H80x80x4-BC-e20-R	341.5	355.1	0.96
H80x80x4-BC-e40	269.6	279.5	0.96
H80x80x4-BC-e80	186.0	194.7	0.95
H80x80x4-BC-e150	127.0	129.1	0.98
Mean			0.98
COV			0.024

Table 4 Comparisons of Test and FE ultimate compression capacities for Short Beam-Columns [2].

Specimens	$P_{Exp,SBC}$ (kN)	$P_{FE,SBC}$ (kN)	$P_{Exp,SBC}/P_{FE,SBC}$
H100x50x4-BC-e0	878.6	863.2	1.02
H100x50x4-BC-e5	738.0	708.8	1.04
H100x50x4-BC-e10	607.9	579.9	1.05
H100x50x4-BC-e25	412.3	396.7	1.04
H100x50x4-BC-e50	251.9	246.9	1.02
H100x50x4-BC-e50-R	255.2	245.3	1.04
H50x100x4-BC-e0	903.2	899.6	1.00
H50x100x4-BC-e8	767.6	763.5	1.01
H50x100x4-BC-e20	632.0	633.9	1.00
H50x100x4-BC-e40	473.2	474.7	1.00
H50x100x4-BC-e100	257.3	264.3	0.97
H200x120x5-BC-e0	1744.7	1898.8	0.92
H200x120x5-BC-e15	1387.8	1408.1	0.99
H200x120x5-BC-e30	1149.4	1170.1	0.98
H200x120x5-BC-e60	821.9	851.2	0.97
H200x120x5-BC-e60-R	825.8	841.6	0.98
H200x120x5-BC-e120	509.4	545.1	0.93
H120x200x5-BC-e0	1701.2	1974.4	0.86
H120x200x5-BC-e15	1602.9	1794.8	0.89
H120x200x5-BC-e30	1451.2	1587.3	0.91
H120x200x5-BC-e60	1243.3	1300.1	0.96
H120x200x5-BC-e110	931.2	968.7	0.96
H120x200x5-BC-e120	931.2	971.9	0.96
H80x80x4-BC-e0	975.6	1022.6	0.95
H80x80x4-BC-e10	754.8	785.7	0.96
H80x80x4-BC-e20	617.9	653.3	0.95
H80x80x4-BC-e40	434.7	458.7	0.95
H80x80x4-BC-e80	282.7	292.8	0.97
H120x120x4-BC-e0	1211.0	1209.3	1.00
H120x120x4-BC-e5	1199.6	1180.9	1.02
H120x120x4-BC-e12	1036.2	1040.5	1.00
H120x120x4-BC-e30	788.2	799.4	0.99
H120x120x4-BC-e60	576.5	583.8	0.99
H120x120x4-BC-e120	365.9	367.1	1.00
V120x120x4-BC-e0	1438.7	1489.1	0.97
V120x120x4-BC-e12	1224.9	1188.6	1.03
V120x120x4-BC-e30	926.2	946.5	0.98
V120x120x4-BC-e60	654.8	667.9	0.98

V120x120x4-BC-e60-R	672.2	675.5	1.00
V120x120x4-BC-e120	393.6	434.8	0.91
V120x120x4-BC-e140	359.0	379.6	0.95
H140x140x6-BC-e0	2434.0	2596.5	0.94
H140x140x6-BC-e15	2035.4	2043.6	1.00
H140x140x6-BC-e35	1612.0	1578.0	1.02
H140x140x6-BC-e70	1141.2	1154.8	0.99
H140x140x6-BC-e100	823.9	915.8	0.90
V80x80x4-BC-e0	1252.2	1342.9	0.93
V80x80x4-BC-e10	995.1	1057.9	0.94
V80x80x4-BC-e20	793.5	785.1	1.01
V80x80x4-BC-e40	588.0	589.9	1.00
V80x80x4-BC-e80	345.6	364.6	0.95
Mean			0.98
COV			0.042

Table 5 Comparisons of test and FE ultimate compression capacities with existing and proposed predicted strengths for Long Beam-Columns.

Specimens	P_u (kN)	P_u / P_{AISC}	P_u / P_{AS}	P_u / P_{EC3}	P_u / P_{pn}
H100x50x4-BC-e0	306.9#	1.03	1.06	1.27	1.08
H100x50x4-BC-e5	241.6#	1.06	1.10	1.14	0.99
H100x50x4-BC-e15	193.6#	1.05	1.10	1.09	0.96
H100x50x4-BC-e30	159.4#	1.02	1.09	1.07	0.94
H100x50x4-BC-e50	128.4#	1.05	1.13	1.09	0.95
H100x50x4-BC-e50-R	129.0#	1.04	1.12	1.08	0.94
H100x50x4-BC-e80	98.7#	1.02	1.11	1.06	0.93
H100x50x4-BC-e130	76.2#	1.04	1.15	1.08	0.94
H50x100x4-BC-e0	642.3#	1.14	1.10	1.35	1.11
H50x100x4-BC-e3	531.6#	1.04	1.03	1.21	1.00
H50x100x4-BC-e10	432.7#	1.03	1.03	1.16	1.00
H50x100x4-BC-e10-R	426.9#	1.04	1.05	1.17	1.00
H50x100x4-BC-e20	364.8#	1.03	1.05	1.15	1.01
H50x100x4-BC-e40	273.6#	1.02	1.06	1.14	1.00
H50x100x4-BC-e80	195.0#	1.05	1.12	1.17	1.02
H50x100x4-BC-e150	132.7#	1.06	1.15	1.19	1.03
H80x80x4-BC-e0	581.9#	1.00	1.02	1.23	1.02
H80x80x4-BC-e5	512.3#	1.06	1.08	1.23	1.03
H80x80x4-BC-e10	422.2#	1.07	1.11	1.22	1.04
H80x80x4-BC-e20	351.9#	1.02	1.07	1.15	0.99
H80x80x4-BC-e20-R	341.5#	1.01	1.06	1.14	0.97
H80x80x4-BC-e40	269.6#	1.01	1.06	1.13	0.96
H80x80x4-BC-e80	186.0#	0.99	1.06	1.10	0.93
H80x80x4-BC-e150	127.0#	1.01	1.09	1.12	0.94
H50x50x4-LBC-e0	55.0	1.12	1.09	1.15	1.06
H50x50x4-LBC-e2	53.5	1.14	1.13	1.13	1.04
H50x50x4-LBC-e5	50.9	1.16	1.15	1.11	1.01
H50x50x4-LBC-e17	45.0	1.17	1.17	1.08	0.98
H50x50x4-LBC-e50	35.9	1.15	1.18	1.07	0.96
H120x120x6-LBC-e0	1141.6	1.09	1.13	1.39	1.14
H120x120x6-LBC-e4	973.6	1.07	1.11	1.26	1.05

H120x120x6-LBC-e12	828.2	1.06	1.10	1.21	1.02
H120x120x6-LBC-e40	604.2	1.05	1.11	1.18	1.00
H120x120x6-LBC-e120	372.4	1.03	1.11	1.15	0.97
H150x150x4-LBC-e0	1179.8	1.10	1.24	1.43	1.19
H150x150x4-LBC-e5	952.8	1.01	1.14	1.25	1.05
H150x150x4-LBC-e15	795.3	1.01	1.13	1.20	1.03
H150x150x4-LBC-e50	547.9	1.01	1.15	1.17	1.01
H150x150x4-LBC-e150	311.5	1.02	1.17	1.17	1.00
H250x250x4-LBC-e0	1311.8	0.94	1.14	1.03	0.97
H250x250x4-LBC-e8	1195.0	0.92	1.12	1.01	0.95
H250x250x4-LBC-e25	1042.8	0.91	1.11	1.01	0.95
H250x250x4-LBC-e83	742.5	0.91	1.11	1.02	0.96
H250x250x4-LBC-e250	418.1	0.92	1.12	1.03	0.98
H300x300x3-LBC-e0	856.7	1.02	1.29	1.06	1.04
H300x300x3-LBC-e10	786.7	0.99	1.25	1.04	1.01
H300x300x3-LBC-e30	691.1	0.95	1.21	1.05	1.00
H300x300x3-LBC-e100	493.7	0.90	1.13	1.06	0.99
H300x300x3-LBC-e300	275.6	0.85	1.05	1.09	0.97
V50x50x4-LBC-e0	52.4	1.13	1.07	1.13	1.05
V50x50x4-LBC-e2	51.4	1.15	1.11	1.12	1.04
V50x50x4-LBC-e5	49.5	1.17	1.13	1.10	1.02
V50x50x4-LBC-e17	45.2	1.19	1.17	1.08	1.00
V50x50x4-LBC-e50	37.9	1.19	1.19	1.07	0.98
V120x120x6-LBC-e0	1177.1	1.07	1.11	1.35	1.13
V120x120x6-LBC-e4	1046.7	1.09	1.13	1.26	1.06
V120x120x6-LBC-e12	910.2	1.09	1.13	1.21	1.03
V120x120x6-LBC-e40	685.1	1.07	1.13	1.18	1.01
V120x120x6-LBC-e120	440.3	1.05	1.12	1.15	0.99
V150x150x4-LBC-e0	1199.2	0.97	1.10	1.29	1.06
V150x150x4-LBC-e5	1051.5	0.97	1.10	1.22	1.02
V150x150x4-LBC-e15	884.1	0.98	1.10	1.17	1.00
V150x150x4-LBC-e50	619.2	0.98	1.11	1.13	0.99
V150x150x4-LBC-e150	361.3	0.98	1.13	1.11	0.99
V250x250x4-LBC-e0	1563.0	0.92	1.12	1.02	0.95
V250x250x4-LBC-e8	1400.2	0.89	1.08	0.98	0.92
V250x250x4-LBC-e25	1202.0	0.87	1.05	0.96	0.91
V250x250x4-LBC-e83	862.7	0.86	1.04	0.96	0.93
V250x250x4-LBC-e250	488.3	0.86	1.04	0.96	0.95
V300x300x3-LBC-e0	1021.5	1.00	1.26	1.05	1.02
V300x300x3-LBC-e10	928.9	0.96	1.20	1.02	0.98
V300x300x3-LBC-e30	811.6	0.92	1.15	1.02	0.97
V300x300x3-LBC-e100	577.3	0.85	1.05	1.02	0.95
V300x300x3-LBC-e300	326.2	0.79	0.97	1.05	0.95
S50x50x4-LBC-e0	51.6	1.13	1.05	1.12	1.05
S50x50x4-LBC-e2	50.6	1.15	1.09	1.11	1.03
S50x50x4-LBC-e5	48.7	1.16	1.11	1.09	1.01
S50x50x4-LBC-e17	44.7	1.17	1.15	1.06	0.98
S50x50x4-LBC-e50	37.8	1.18	1.17	1.05	0.96
S120x120x6-LBC-e0	1151.8	1.04	1.07	1.31	1.10
S120x120x6-LBC-e4	1037.5	1.08	1.10	1.23	1.05
S120x120x6-LBC-e12	913.3	1.08	1.12	1.19	1.02
S120x120x6-LBC-e40	701.8	1.08	1.13	1.16	1.01
S120x120x6-LBC-e120	463.9	1.06	1.14	1.16	1.02
S150x150x4-LBC-e0	1166.2	0.91	1.04	1.23	1.00
S150x150x4-LBC-e5	1032.6	0.93	1.05	1.16	0.97

S150x150x4-LBC-e15	880.8	0.94	1.06	1.13	0.97
S150x150x4-LBC-e50	627.7	0.95	1.08	1.10	0.97
S150x150x4-LBC-e150	374.5	0.97	1.12	1.10	0.99
S250x250x4-LBC-e0	1640.6	0.93	1.12	1.02	0.95
S250x250x4-LBC-e8	1457.5	0.88	1.07	0.97	0.91
S250x250x4-LBC-e25	1249.2	0.86	1.03	0.95	0.90
S250x250x4-LBC-e83	902.1	0.86	1.03	0.95	0.93
S250x250x4-LBC-e250	518.1	0.86	1.03	0.96	0.96
S300x300x3-LBC-e0	1082.6	1.02	1.27	1.06	1.03
S300x300x3-LBC-e10	975.6	0.96	1.20	1.02	0.98
S300x300x3-LBC-e30	851.0	0.92	1.14	1.02	0.97
S300x300x3-LBC-e100	608.4	0.85	1.05	1.03	0.95
S300x300x3-LBC-e300	346.8	0.79	0.97	1.06	0.96
H60x40x3-LBC-e0	31.3	1.12	1.08	1.13	1.05
H60x40x3-LBC-e1	30.8	1.14	1.12	1.12	1.04
H60x40x3-LBC-e4	29.5	1.15	1.13	1.09	1.01
H60x40x3-LBC-e13	26.7	1.16	1.15	1.05	0.97
H60x40x3-LBC-e40	22.2	1.15	1.16	1.02	0.92
H120x80x4-LBC-e0	363.4	1.11	1.15	1.33	1.14
H120x80x4-LBC-e3	323.9	1.12	1.16	1.23	1.05
H120x80x4-LBC-e8	288.2	1.12	1.17	1.17	1.00
H120x80x4-LBC-e27	226.6	1.12	1.18	1.13	0.96
H120x80x4-LBC-e80	153.4	1.11	1.19	1.12	0.93
H200x100x3-LBC-e0	424.6	0.79	0.90	1.06	0.86
H200x100x3-LBC-e3	387.8	0.83	0.94	1.03	0.85
H200x100x3-LBC-e10	337.7	0.86	0.97	1.01	0.85
H200x100x3-LBC-e33	251.6	0.90	1.03	1.02	0.88
H200x100x3-LBC-e100	157.9	0.94	1.12	1.06	0.92
H300x200x3-LBC-e0	788.1	0.98	1.22	1.08	1.01
H300x200x3-LBC-e7	704.0	0.94	1.17	1.03	0.97
H300x200x3-LBC-e20	611.9	0.92	1.14	1.01	0.96
H300x200x3-LBC-e67	444.1	0.92	1.14	1.02	0.98
H300x200x3-LBC-e200	255.5	0.92	1.14	1.04	1.00
H40x60x3-LBC-e0	59.0	1.12	1.10	1.19	1.08
H40x60x3-LBC-e2	56.7	1.15	1.14	1.16	1.05
H40x60x3-LBC-e6	53.0	1.16	1.16	1.13	1.02
H40x60x3-LBC-e20	45.3	1.16	1.18	1.10	0.98
H40x60x3-LBC-e60	34.2	1.13	1.17	1.09	0.97
H80x120x4-LBC-e0	609.4	1.09	1.14	1.40	1.15
H80x120x4-LBC-e4	520.4	1.07	1.12	1.26	1.05
H80x120x4-LBC-e12	442.0	1.06	1.11	1.19	1.00
H80x120x4-LBC-e40	321.7	1.05	1.11	1.19	1.02
H80x120x4-LBC-e120	196.8	1.03	1.11	1.15	0.98
H100x200x3-LBC-e0	714.1	1.02	1.18	1.21	1.07
H100x200x3-LBC-e7	642.5	1.00	1.15	1.17	1.04
H100x200x3-LBC-e20	555.9	1.00	1.15	1.16	1.04
H100x200x3-LBC-e67	392.3	1.01	1.16	1.16	1.04
H100x200x3-LBC-e200	217.3	0.99	1.14	1.14	1.01
H200x300x3-LBC-e0	810.1	0.99	1.23	1.04	1.01
H200x300x3-LBC-e10	743.3	0.96	1.19	1.03	0.99
H200x300x3-LBC-e30	650.1	0.93	1.15	1.03	0.98
H200x300x3-LBC-e100	464.4	0.89	1.09	1.05	0.97
H200x300x3-LBC-e300	255.1	0.83	1.01	1.05	0.94
V60x40x3-LBC-e0	29.9	1.12	1.05	1.10	1.04
V60x40x3-LBC-e1	29.5	1.14	1.09	1.09	1.03

V60x40x3-LBC-e4	28.6	1.15	1.10	1.07	1.01
V60x40x3-LBC-e13	26.5	1.16	1.13	1.04	0.97
V60x40x3-LBC-e40	23.0	1.17	1.16	1.02	0.94
V120x80x4-LBC-e0	353.1	1.12	1.11	1.28	1.12
V120x80x4-LBC-e3	323.7	1.14	1.14	1.20	1.05
V120x80x4-LBC-e8	295.4	1.15	1.17	1.16	1.01
V120x80x4-LBC-e27	240.4	1.15	1.19	1.11	0.97
V120x80x4-LBC-e80	169.5	1.13	1.20	1.09	0.94
V200x100x3-LBC-e0	424.5	0.70	0.82	0.98	0.80
V200x100x3-LBC-e3	395.2	0.77	0.87	0.96	0.80
V200x100x3-LBC-e10	352.8	0.80	0.91	0.95	0.81
V200x100x3-LBC-e33	271.5	0.85	0.98	0.96	0.84
V200x100x3-LBC-e100	176.5	0.90	1.06	1.00	0.89
V300x200x3-LBC-e0	912.6	0.94	1.17	1.05	0.97
V300x200x3-LBC-e7	803.6	0.89	1.10	0.99	0.92
V300x200x3-LBC-e20	696.0	0.86	1.06	0.98	0.91
V300x200x3-LBC-e67	507.0	0.86	1.05	1.00	0.93
V300x200x3-LBC-e200	295.2	0.86	1.05	1.04	0.96
V40x60x3-LBC-e0	56.3	1.12	1.07	1.15	1.06
V40x60x3-LBC-e2	54.7	1.15	1.12	1.13	1.04
V40x60x3-LBC-e6	52.0	1.17	1.14	1.11	1.02
V40x60x3-LBC-e20	46.2	1.18	1.17	1.09	0.99
V40x60x3-LBC-e60	36.8	1.17	1.18	1.08	0.98
V80x120x4-LBC-e0	625.1	1.08	1.12	1.37	1.14
V80x120x4-LBC-e4	557.1	1.10	1.14	1.27	1.07
V80x120x4-LBC-e12	484.5	1.10	1.14	1.20	1.02
V80x120x4-LBC-e40	364.5	1.08	1.14	1.20	1.04
V80x120x4-LBC-e120	232.5	1.04	1.12	1.15	1.01
V100x200x3-LBC-e0	839.8	1.00	1.16	1.21	1.04
V100x200x3-LBC-e7	753.3	0.98	1.13	1.16	1.02
V100x200x3-LBC-e20	652.1	0.98	1.13	1.15	1.02
V100x200x3-LBC-e67	459.2	0.97	1.11	1.13	1.02
V100x200x3-LBC-e200	248.4	0.91	1.05	1.06	0.96
V200x300x3-LBC-e0	962.9	0.97	1.20	1.03	0.98
V200x300x3-LBC-e10	874.1	0.93	1.15	1.00	0.95
V200x300x3-LBC-e30	763.7	0.89	1.10	1.00	0.94
V200x300x3-LBC-e100	547.7	0.85	1.03	1.02	0.94
V200x300x3-LBC-e300	301.4	0.78	0.94	1.02	0.91
S60x40x3-LBC-e0	29.4	1.12	1.03	1.10	1.03
S60x40x3-LBC-e1	29.1	1.14	1.07	1.09	1.02
S60x40x3-LBC-e4	28.1	1.14	1.08	1.06	1.00
S60x40x3-LBC-e13	26.0	1.14	1.11	1.03	0.96
S60x40x3-LBC-e40	22.7	1.15	1.13	1.00	0.93
S120x80x4-LBC-e0	348.6	1.12	1.09	1.26	1.11
S120x80x4-LBC-e3	316.7	1.12	1.11	1.17	1.03
S120x80x4-LBC-e8	289.9	1.13	1.14	1.13	0.99
S120x80x4-LBC-e27	237.4	1.13	1.16	1.08	0.95
S120x80x4-LBC-e80	170.0	1.12	1.18	1.06	0.93
S200x100x3-LBC-e0	413.0	0.67	0.78	0.94	0.77
S200x100x3-LBC-e3	386.2	0.74	0.83	0.92	0.77
S200x100x3-LBC-e10	347.0	0.78	0.88	0.92	0.78
S200x100x3-LBC-e33	270.8	0.83	0.95	0.93	0.82
S200x100x3-LBC-e100	179.4	0.88	1.03	0.97	0.87
S300x200x3-LBC-e0	934.5	0.92	1.14	1.03	0.94
S300x200x3-LBC-e7	819.9	0.86	1.07	0.97	0.89

S300x200x3-LBC-e20	712.5	0.84	1.03	0.96	0.88
S300x200x3-LBC-e67	522.7	0.84	1.02	0.99	0.91
S300x200x3-LBC-e200	308.3	0.84	1.03	1.03	0.95
S40x60x3-LBC-e0	55.5	1.12	1.05	1.14	1.06
S40x60x3-LBC-e2	53.8	1.14	1.10	1.12	1.03
S40x60x3-LBC-e6	51.3	1.15	1.12	1.10	1.01
S40x60x3-LBC-e20	45.7	1.17	1.15	1.07	0.98
S40x60x3-LBC-e60	37.0	1.16	1.16	1.06	0.96
S80x120x4-LBC-e0	610.5	1.05	1.09	1.32	1.12
S80x120x4-LBC-e4	551.3	1.09	1.12	1.24	1.05
S80x120x4-LBC-e12	485.1	1.09	1.13	1.18	1.01
S80x120x4-LBC-e40	373.0	1.08	1.14	1.18	1.04
S80x120x4-LBC-e120	243.5	1.05	1.13	1.15	1.03
S100x200x3-LBC-e0	862.4	0.98	1.14	1.19	1.03
S100x200x3-LBC-e7	773.0	0.96	1.11	1.15	1.00
S100x200x3-LBC-e20	667.5	0.96	1.10	1.13	1.00
S100x200x3-LBC-e67	470.9	0.95	1.09	1.11	1.00
S100x200x3-LBC-e200	257.6	0.89	1.03	1.05	0.95
S200x300x3-LBC-e0	1017.9	0.98	1.21	1.04	0.99
S200x300x3-LBC-e10	917.1	0.93	1.14	1.00	0.95
S200x300x3-LBC-e30	797.9	0.89	1.09	1.00	0.94
S200x300x3-LBC-e100	577.4	0.85	1.03	1.03	0.94
S200x300x3-LBC-e300	322.0	0.78	0.94	1.04	0.93
No. of Data (n)		219	219	219	219
Mean (P_m)		1.01	1.10	1.11	0.99
COV (V_P)		0.114	0.068	0.088	0.068
Resistance Factor (ϕ)		0.90	0.90	1.00	0.85
Reliability Index (β_0)		2.38	2.68	2.27	2.52

Note: # denotes data from Ma et al. [1].

Table 6 Comparisons of test and FE ultimate compression capacities with existing and proposed predicted strengths for Short Beam-Columns.

Specimens	P_u (kN)	P_u / P_{AISC}	P_u / P_{AS}	P_u / P_{EC3}	P_u / P_{pn}
H100x50x4-BC-e0	878.6*	1.19	1.18	1.24	1.18
H100x50x4-BC-e5	738.0*	1.20	1.21	1.21	1.13
H100x50x4-BC-e10	607.9*	1.21	1.25	1.32	1.15
H100x50x4-BC-e25	412.3*	1.20	1.28	1.19	1.06
H100x50x4-BC-e50	251.9*	1.17	1.28	1.17	1.02
H100x50x4-BC-e50-R	255.2*	1.19	1.31	1.38	1.08
H50x100x4-BC-e0	903.2*	1.18	1.17	1.17	1.17
H50x100x4-BC-e8	767.6*	1.24	1.26	1.26	1.21
H50x100x4-BC-e20	632.0*	1.28	1.33	1.21	1.14
H50x100x4-BC-e40	473.2*	1.32	1.40	1.26	1.16
H50x100x4-BC-e100	257.3*	1.28	1.40	1.29	1.13
H120x200x5-BC-e0	1701.2*	0.93	0.98	0.94	0.94
H120X200X5-BC-e15	1602.9*	1.02	1.09	1.04	1.02
H120x200x5-BC-e30	1451.2*	1.07	1.16	1.10	1.07
H120x200x5-BC-e60	1243.3*	1.14	1.26	1.19	1.14
H120x200x5-BC-e110	931.2*	1.16	1.30	1.23	1.16
H120x200x5-BC-e110	931.2*	1.16	1.29	1.23	1.15
H200x120x5-BC-e0	1744.7*	0.95	1.00	0.96	0.96
H200x120x5-BC-e15	1387.8*	1.02	1.12	1.07	1.01
H200x120x5-BC-e30	1149.4*	1.03	1.15	1.10	1.01

H200x120x5-BC-e60	821.9*	1.03	1.18	1.12	1.00
H200x120x5-BC-e60-R	825.8*	1.05	1.20	1.14	1.02
H200x120x5-BC-e120	509.4*	1.01	1.18	1.12	0.97
H80x80x4-BC-e0	975.6*	1.11	1.10	1.11	1.09
H80x80x4-BC-e10	754.8*	1.13	1.16	1.11	1.04
H80x80x4-BC-e20	617.9*	1.12	1.17	1.10	1.01
H80x80x4-BC-e40	434.7*	1.12	1.20	1.12	0.98
H80x80x4-BC-e80	282.7*	1.13	1.23	1.17	0.98
H120x120x4-BC-e0	1211.0*	1.04	1.09	1.09	1.08
H120x120x4-BC-e5	1199.6*	1.13	1.19	1.18	1.16
H120x120x4-BC-e12	1036.2*	1.14	1.21	1.21	1.15
H120x120x4-BC-e30	788.2*	1.15	1.26	1.25	1.13
H120x120x4-BC-e60	576.5*	1.17	1.29	1.29	1.12
H120x120x4-BC-e120	365.9*	1.18	1.33	1.33	1.11
H140x140x6-BC-e0	2434.0*	1.19	1.18	1.18	1.18
H140x140x6-BC-e15	2035.4*	1.24	1.27	1.20	1.16
H140x140x6-BC-e35	1612.0*	1.28	1.35	1.25	1.15
H140x140x6-BC-e70	1141.2*	1.24	1.34	1.22	1.09
H140x140x6-BC-e100	823.9*	1.12	1.23	1.13	0.98
V80x80x4-BC-e0	1252.2*	1.14	1.13	1.14	1.11
V80x80x4-BC-e10	995.1*	1.12	1.14	1.11	1.05
V80x80x4-BC-e20	793.5*	1.20	1.26	1.19	1.09
V80x80x4-BC-e40	588.0*	1.17	1.25	1.18	1.05
V80x80x4-BC-e80	345.6*	1.09	1.19	1.13	0.98
V120x120x4-BC-e0	1438.7*	0.97	1.03	0.99	0.99
V120x120x4-BC-e12	1224.9*	1.08	1.17	1.13	1.08
V120x120x4-BC-e30	926.2*	1.04	1.15	1.11	1.04
V120x120x4-BC-e60	654.8*	1.06	1.19	1.15	1.04
V120x120x4-BC-e60-R	672.2*	1.07	1.20	1.17	1.06
V120x120x4-BC-e120	393.6*	0.98	1.11	1.08	0.96
V120x120x4-BC-e140	359.0*	1.01	1.16	1.13	0.99
H50x50x4-SBC-e0	437.2	1.17	1.14	1.33	1.12
H50x50x4-SBC-e2	316.5	1.13	1.14	1.26	1.08
H50x50x4-SBC-e5	257.8	1.13	1.16	1.25	1.08
H50x50x4-SBC-e17	193.3	1.14	1.19	1.25	1.08
H50x50x4-SBC-e50	130.6	1.14	1.22	1.25	1.07
H120x120x6-SBC-e0	2165.8	1.20	1.19	1.22	1.18
H120x120x6-SBC-e4	1651.1	1.20	1.23	1.20	1.11
H120x120x6-SBC-e12	1352.3	1.22	1.27	1.22	1.10
H120x120x6-SBC-e40	994.1	1.23	1.31	1.25	1.09
H120x120x6-SBC-e120	639.8	1.22	1.33	1.28	1.07
H150x150x4-SBC-e0	1197.3	0.91	1.01	0.95	0.94
H150x150x4-SBC-e5	1008.7	1.02	1.16	1.09	1.03
H150x150x4-SBC-e15	826.0	1.04	1.19	1.13	1.05
H150x150x4-SBC-e50	604.7	1.06	1.23	1.17	1.05
H150x150x4-SBC-e150	389.0	1.07	1.25	1.19	1.04
H250x250x4-SBC-e0	1429.5	0.98	1.20	1.01	1.01
H250x250x4-SBC-e8	1191.8	1.03	1.26	1.08	1.07
H250x250x4-SBC-e25	955.3	1.00	1.22	1.06	1.04
H250x250x4-SBC-e83	702.6	0.98	1.20	1.06	1.03
H250x250x4-SBC-e250	464.6	0.98	1.20	1.08	1.04
H300x300x3-SBC-e0	922.8	1.08	1.37	1.10	1.10
H300x300x3-SBC-e10	741.2	1.04	1.31	1.13	1.09
H300x300x3-SBC-e30	618.5	1.01	1.27	1.15	1.09
H300x300x3-SBC-e100	464.5	0.97	1.21	1.17	1.08

H300x300x3-SBC-e300	306.4	0.92	1.14	1.18	1.06
V50x50x4-SBC-e0	531.5	1.19	1.16	1.40	1.16
V50x50x4-SBC-e2	374.7	1.13	1.14	1.28	1.09
V50x50x4-SBC-e5	305.0	1.12	1.15	1.26	1.08
V50x50x4-SBC-e17	230.3	1.12	1.17	1.25	1.08
V50x50x4-SBC-e50	158.0	1.11	1.18	1.24	1.06
V120x120x6-SBC-e0	2873.9	1.20	1.18	1.24	1.18
V120x120x6-SBC-e4	2128.5	1.17	1.19	1.19	1.10
V120x120x6-SBC-e12	1719.1	1.17	1.22	1.19	1.07
V120x120x6-SBC-e40	1247.2	1.17	1.24	1.20	1.06
V120x120x6-SBC-e120	800.5	1.15	1.25	1.21	1.04
V150x150x4-SBC-e0	1423.2	0.88	0.98	0.91	0.90
V150x150x4-SBC-e5	1187.0	0.97	1.10	1.02	0.98
V150x150x4-SBC-e15	983.2	0.99	1.14	1.07	1.01
V150x150x4-SBC-e50	726.2	1.01	1.18	1.11	1.03
V150x150x4-SBC-e150	469.1	1.01	1.19	1.13	1.03
V250x250x4-SBC-e0	1738.1	0.98	1.19	0.99	0.99
V250x250x4-SBC-e8	1369.0	0.96	1.16	0.99	1.00
V250x250x4-SBC-e25	1138.2	0.95	1.16	1.00	1.01
V250x250x4-SBC-e83	845.3	0.94	1.14	1.01	1.01
V250x250x4-SBC-e250	557.2	0.92	1.12	1.01	1.02
V300x300x3-SBC-e0	1105.5	1.06	1.34	1.08	1.08
V300x300x3-SBC-e10	859.1	0.98	1.22	1.07	1.03
V300x300x3-SBC-e30	727.6	0.96	1.19	1.10	1.05
V300x300x3-SBC-e100	540.2	0.90	1.11	1.11	1.03
V300x300x3-SBC-e300	362.4	0.86	1.05	1.13	1.03
S50x50x4-SBC-e0	547.1	1.17	1.14	1.39	1.14
S50x50x4-SBC-e2	394.7	1.13	1.15	1.29	1.10
S50x50x4-SBC-e5	325.5	1.13	1.17	1.28	1.10
S50x50x4-SBC-e17	248.8	1.14	1.19	1.28	1.10
S50x50x4-SBC-e50	173.1	1.14	1.21	1.27	1.09
S120x120x6-SBC-e0	3351.8	1.29	1.27	1.34	1.26
S120x120x6-SBC-e4	2390.2	1.21	1.24	1.24	1.14
S120x120x6-SBC-e12	1929.2	1.21	1.27	1.24	1.13
S120x120x6-SBC-e40	1388.3	1.20	1.28	1.24	1.10
S120x120x6-SBC-e120	887.9	1.18	1.29	1.24	1.09
S150x150x4-SBC-e0	1523.2	0.89	1.00	0.92	0.91
S150x150x4-SBC-e5	1251.5	0.96	1.10	1.02	0.98
S150x150x4-SBC-e15	1041.3	0.99	1.14	1.06	1.01
S150x150x4-SBC-e50	772.6	1.02	1.18	1.11	1.04
S150x150x4-SBC-e150	507.9	1.03	1.21	1.14	1.06
S250x250x4-SBC-e0	1879.7	1.01	1.22	1.02	1.02
S250x250x4-SBC-e8	1475.1	0.98	1.19	1.01	1.02
S250x250x4-SBC-e25	1224.9	0.97	1.18	1.02	1.03
S250x250x4-SBC-e83	913.6	0.96	1.16	1.02	1.04
S250x250x4-SBC-e250	601.1	0.94	1.14	1.02	1.04
S300x300x3-SBC-e0	1186.9	1.09	1.37	1.10	1.10
S300x300x3-SBC-e10	938.3	1.02	1.27	1.10	1.07
S300x300x3-SBC-e30	790.6	0.99	1.22	1.13	1.08
S300x300x3-SBC-e100	593.2	0.93	1.15	1.15	1.07
S300x300x3-SBC-e300	380.3	0.85	1.04	1.12	1.02
H60x40x3-SBC-e0	290.5	1.11	1.09	1.30	1.07
H60x40x3-SBC-e1	215.0	1.07	1.09	1.22	1.03
H60x40x3-SBC-e4	177.4	1.07	1.10	1.20	1.02
H60x40x3-SBC-e13	135.6	1.07	1.12	1.19	1.01

H60x40x3-SBC-e40	94.3	1.07	1.14	1.19	0.99
H120x80x4-SBC-e0	1046.1	1.09	1.11	1.19	1.11
H120x80x4-SBC-e3	771.8	1.08	1.14	1.19	1.06
H120x80x4-SBC-e8	623.2	1.09	1.17	1.22	1.06
H120x80x4-SBC-e27	453.9	1.10	1.21	1.24	1.05
H120x80x4-SBC-e80	296.3	1.11	1.24	1.27	1.04
H200x100x3-SBC-e0	758.7	1.00	1.15	1.06	1.04
H200x100x3-SBC-e3	588.9	1.02	1.20	1.09	1.03
H200x100x3-SBC-e10	483.0	1.04	1.24	1.12	1.04
H200x100x3-SBC-e33	357.7	1.06	1.28	1.16	1.05
H200x100x3-SBC-e100	235.4	1.07	1.32	1.20	1.06
H300x200x3-SBC-e0	877.3	1.05	1.31	1.07	1.07
H300x200x3-SBC-e7	708.4	1.04	1.30	1.09	1.08
H300x200x3-SBC-e20	597.6	1.05	1.31	1.11	1.10
H300x200x3-SBC-e67	445.8	1.03	1.29	1.11	1.10
H300x200x3-SBC-e200	296.0	1.02	1.27	1.12	1.10
H40x60x3-SBC-e0	364.8	1.16	1.13	1.29	1.12
H40x60x3-SBC-e2	265.2	1.14	1.15	1.23	1.08
H40x60x3-SBC-e6	215.3	1.15	1.18	1.24	1.08
H40x60x3-SBC-e20	159.3	1.16	1.22	1.25	1.08
H40x60x3-SBC-e60	105.2	1.15	1.24	1.25	1.07
H80x120x4-SBC-e0	1142.8	1.15	1.17	1.21	1.16
H80x120x4-SBC-e4	888.9	1.18	1.23	1.26	1.17
H80x120x4-SBC-e12	731.5	1.21	1.28	1.31	1.18
H80x120x4-SBC-e40	518.6	1.19	1.28	1.30	1.14
H80x120x4-SBC-e120	335.4	1.19	1.30	1.24	1.06
H100x200x3-SBC-e0	763.8	0.99	1.14	1.02	1.02
H100x200x3-SBC-e7	612.5	1.02	1.17	1.07	1.04
H100x200x3-SBC-e20	507.0	1.02	1.18	1.09	1.04
H100x200x3-SBC-e67	373.9	1.02	1.18	1.11	1.03
H100x200x3-SBC-e200	238.3	0.99	1.14	1.09	0.99
H200x300x3-SBC-e0	867.8	1.03	1.29	1.06	1.06
H200x300x3-SBC-e10	699.1	1.01	1.25	1.09	1.06
H200x300x3-SBC-e30	575.6	0.97	1.20	1.10	1.04
H200x300x3-SBC-e100	421.1	0.92	1.13	1.10	1.01
H200x300x3-SBC-e300	274.2	0.87	1.06	1.09	0.98
V60x40x3-SBC-e0	338.7	1.12	1.12	1.35	1.10
V60x40x3-SBC-e1	250.4	1.08	1.11	1.24	1.04
V60x40x3-SBC-e4	207.8	1.07	1.11	1.21	1.03
V60x40x3-SBC-e13	160.5	1.06	1.12	1.19	1.01
V60x40x3-SBC-e40	113.6	1.05	1.12	1.17	0.99
V120x80x4-SBC-e0	1286.0	1.06	1.09	1.17	1.07
V120x80x4-SBC-e3	934.4	1.04	1.11	1.16	1.04
V120x80x4-SBC-e8	748.5	1.05	1.13	1.17	1.03
V120x80x4-SBC-e27	544.6	1.05	1.17	1.19	1.03
V120x80x4-SBC-e80	354.5	1.06	1.19	1.20	1.02
V200x100x3-SBC-e0	879.9	0.94	1.09	1.00	0.97
V200x100x3-SBC-e3	703.9	0.99	1.17	1.06	1.01
V200x100x3-SBC-e10	583.7	1.01	1.21	1.09	1.03
V200x100x3-SBC-e33	429.6	1.02	1.23	1.12	1.03
V200x100x3-SBC-e100	285.6	1.04	1.27	1.15	1.05
V300x200x3-SBC-e0	1048.3	1.03	1.27	1.04	1.04
V300x200x3-SBC-e7	847.9	1.02	1.26	1.08	1.05
V300x200x3-SBC-e20	698.6	0.99	1.22	1.08	1.05
V300x200x3-SBC-e67	524.0	0.97	1.20	1.10	1.05

V300x200x3-SBC-e200	351.4	0.96	1.18	1.13	1.06
V40x60x3-SBC-e0	456.5	1.17	1.13	1.34	1.12
V40x60x3-SBC-e2	321.8	1.12	1.13	1.24	1.07
V40x60x3-SBC-e6	260.0	1.12	1.15	1.23	1.07
V40x60x3-SBC-e20	193.5	1.12	1.17	1.24	1.07
V40x60x3-SBC-e60	129.2	1.11	1.19	1.23	1.05
V80x120x4-SBC-e0	1433.9	1.12	1.16	1.19	1.14
V80x120x4-SBC-e4	1130.5	1.17	1.23	1.26	1.17
V80x120x4-SBC-e12	928.3	1.18	1.26	1.29	1.18
V80x120x4-SBC-e40	683.1	1.20	1.29	1.32	1.19
V80x120x4-SBC-e120	421.0	1.13	1.24	1.25	1.11
V100x200x3-SBC-e0	911.1	0.96	1.11	0.98	0.98
V100x200x3-SBC-e7	711.2	0.95	1.09	0.99	0.97
V100x200x3-SBC-e20	587.6	0.94	1.09	1.01	0.97
V100x200x3-SBC-e67	433.0	0.93	1.08	1.02	0.97
V100x200x3-SBC-e200	279.6	0.90	1.05	1.02	0.95
V200x300x3-SBC-e0	1046.9	1.02	1.27	1.04	1.04
V200x300x3-SBC-e10	844.6	0.99	1.22	1.07	1.04
V200x300x3-SBC-e30	684.5	0.93	1.14	1.06	1.01
V200x300x3-SBC-e100	501.6	0.87	1.06	1.06	0.98
V200x300x3-SBC-e300	329.6	0.82	1.00	1.07	0.96
S60x40x3-SBC-e0	341.0	1.09	1.09	1.32	1.08
S60x40x3-SBC-e1	258.3	1.08	1.11	1.23	1.04
S60x40x3-SBC-e4	216.7	1.08	1.12	1.21	1.04
S60x40x3-SBC-e13	169.5	1.07	1.13	1.20	1.03
S60x40x3-SBC-e40	121.5	1.06	1.14	1.19	1.02
S120x80x4-SBC-e0	1356.5	1.05	1.08	1.17	1.06
S120x80x4-SBC-e3	990.1	1.04	1.11	1.16	1.03
S120x80x4-SBC-e8	799.1	1.05	1.14	1.18	1.04
S120x80x4-SBC-e27	584.6	1.07	1.18	1.20	1.04
S120x80x4-SBC-e80	385.4	1.08	1.22	1.22	1.05
S200x100x3-SBC-e0	935.9	0.95	1.10	1.01	0.98
S200x100x3-SBC-e3	749.9	1.00	1.18	1.07	1.02
S200x100x3-SBC-e10	624.2	1.02	1.22	1.10	1.04
S200x100x3-SBC-e33	466.4	1.05	1.26	1.14	1.06
S200x100x3-SBC-e100	311.2	1.07	1.31	1.18	1.09
S300x200x3-SBC-e0	1125.4	1.05	1.30	1.06	1.06
S300x200x3-SBC-e7	910.6	1.04	1.28	1.10	1.07
S300x200x3-SBC-e20	757.3	1.02	1.25	1.11	1.08
S300x200x3-SBC-e67	561.4	0.98	1.21	1.12	1.07
S300x200x3-SBC-e200	377.9	0.97	1.19	1.15	1.08
S40x60x3-SBC-e0	484.6	1.17	1.13	1.35	1.13
S40x60x3-SBC-e2	346.8	1.14	1.15	1.27	1.10
S40x60x3-SBC-e6	283.1	1.15	1.17	1.27	1.10
S40x60x3-SBC-e20	212.5	1.15	1.21	1.28	1.11
S40x60x3-SBC-e60	143.4	1.15	1.23	1.27	1.10
S80x120x4-SBC-e0	1584.2	1.16	1.20	1.24	1.17
S80x120x4-SBC-e4	1256.9	1.21	1.28	1.31	1.22
S80x120x4-SBC-e12	1039.0	1.23	1.33	1.34	1.24
S80x120x4-SBC-e40	767.8	1.25	1.36	1.37	1.26
S80x120x4-SBC-e120	462.2	1.15	1.28	1.27	1.15
S100x200x3-SBC-e0	960.4	0.96	1.11	0.97	0.97
S100x200x3-SBC-e7	759.2	0.96	1.11	1.00	0.98
S100x200x3-SBC-e20	627.1	0.95	1.10	1.02	0.98
S100x200x3-SBC-e67	462.2	0.93	1.08	1.03	0.98

S100x200x3-SBC-e200	300.0	0.91	1.06	1.03	0.96
S200x300x3-SBC-e0	1123.5	1.05	1.30	1.06	1.06
S200x300x3-SBC-e10	905.1	1.00	1.23	1.09	1.06
S200x300x3-SBC-e30	738.7	0.95	1.16	1.09	1.03
S200x300x3-SBC-e100	540.5	0.88	1.08	1.08	1.00
S200x300x3-SBC-e300	355.7	0.83	1.01	1.09	0.98
No. of Data (n)		246	246	246	246
Mean (P_m)		1.07	1.19	1.16	1.06
COV (V_P)		0.092	0.068	0.086	0.058
Resistance Factor (ϕ)		0.90	0.90	1.00	0.90
Reliability Index (β_0)		2.69	2.98	2.45	2.61

Note: * denotes data from Ma et al. [2].

Table 7 Summary of comparisons of test and FE ultimate capacities with existing and proposed predicted strengths

No. of		$\frac{P_u}{P_{AISC}}$	$\frac{P_u}{P_{AS}}$	$\frac{P_u}{P_{EC3}}$	$\frac{P_u}{P_{pn}}$
Tests:75	FE:390				
LBC: 219	Mean	1.01	1.10	1.11	0.99
	COV	0.114	0.068	0.088	0.068
SBC: 246	Mean	1.07	1.19	1.16	1.06
	COV	0.092	0.067	0.086	0.058
ALL: 465	Mean	1.04	1.15	1.13	1.03
	COV	0.106	0.077	0.090	0.072
	ϕ	0.90	0.90	1.00	1.00
	β_0	2.53	2.81	2.36	2.02
	$\phi^{\#}$	0.85	0.85	0.85	0.85
	$\beta_0{}^{\#}$	2.75	3.04	3.00	2.67

#Reliability analysis using resistance factor of 0.85

LBC: Long beam-columns

SBC: Short beam-columns